Feasibility of monitoring Z_{DR} calibration using ground clutter

Report on NPI-2015

Valery Melnikov[*+] with contributions by Dusan Zrnic[+]

[*]- The University of Oklahoma, CIMMS, Norman, OK.

[+] - NOAA/OAR National Severe Storms Laboratory, Norman, OK

October 2015

Contents

1. Introduction

To obtain high quality radar data from clouds and precipitation, radars have to be precisely calibrated. The WSR-88D's system specifications establish uncertainty of ±1 dB and ±0.1 dB for reflectivity (Z) and differential reflectivity (Z_{DR}) estimates. The uncertainties depend on the quality of radar hardware and the statistical properties of returned radar signals. To monitor radar hardware, the WSR-88Ds have built-in equipment and special procedures. Due to variety of factors that affect radar measurements there is no consensus on sufficiency of built-in radar equipment to achieve indicated accuracies. That is why various procedures have been developed to verify radar calibration. All such procedures are based on remote sensing of scatterers that possess certain characteristics. To calibrate Z and Z_{DR}, signal reflected from a metal sphere has been utilized (e.g., Bringi and Chandrasekar 2001, section 6.3.1; Atlas 2002, Williams et al. 2013). The main problem with this approach is its arrangement complexity that leads to the impracticability of routine measurements. Moreover, such measurements give the system gain in one point in the antenna pattern (usually the center of pattern) whereas weather scatterers are distributed and therefore and therefore the shape of antenna pattern needs to be known at least within the mainlobe.

A special procedure for relative Z calibration for adjacent WSR-88D radars has been developed (Zhang et al. 2011). This procedure is applied when adjacent radars observe the same parts of precipitation. Reflectivity estimates from these radars should be equal, if not adjustment can be made for these to agree. However, bringing reflectivity to the same level does not guarantee the correct absolute Z calibration, which remains one of the major problems in radar meteorology.

Vertical sensing of precipitation is used in some radars to calibrate Z_{DR}. Raindrops appear round in the mean at vertical radar sensing if there is no strong wind shear that can incline/cant the drops relative to radar beam (Gorgucci et al. 1999). This method is used on the German, French, and Finnish weather radar networks (Frech 2013, Sugier and Tabary 2006, Vaisala 2014) but cannot be used on the WSR-88Ds because the maximum elevation angle of their antennas is 60°.

To calibrate Z_{DR} on the WSR-88Ds, built-in equipment and measurement routines have been designed by the manufacturer. To verify calibration, three methods are used operationally (Cunnigham et al. 2013). The first is based on measurements of Z_{DR} in drizzle or light rain. Z_{DR} in drizzle should be close to 0 dB. How close to 0 dB remains unknown because drizzles can contain a small number of large drops that would bias Z_{DR} high. It is assumed that climatological Z_{DR} values in light rain for a given region have certain values which could verify long time calibration. Z_{DR} in a given rain can deviate from the climatological mean and should be used with caution.

The second method to verify Z_{DR} calibration utilizes measurements from snow/crystal cloud areas. It is assumed that snow aggregates exist just above the melting layer and that their Z_{DR} is about 0.2 dB. The problem with this approach is that characteristics of snow/crystal particles above the melting layer are not precisely known hence applicability of this approach to a given

case remains uncertain. Cloud layers with Z_{DR} much larger than 0.2 dB and located just above the melting layer have been observed with the WSR-88Ds.

The third method is based on observations of reflection from clear air. The top of convective boundary layer contains continuum of turbulent eddies including sizes of about 5 cm (half of the radar wavelength) that cause Bragg scatter of S band radiation (Doviak and Zrnic 2006, chapter 11, Hoban et al. 2013). Due to small eddies' sizes and their chaotic spatial orientations in turbulent layers, their Z_{DR} is close to 0 dB (Melnikov et al. 2011). Bragg scatter is easy to observe in cold seasons; in warm months Bragg scatter is often masked by reflections from insects. Nevertheless, operational radar observations show sufficient detectability of Bragg scatter year round on almost all radar sites (Cunnigham et al. 2013, Hoban et al. 2013, Ice et al. 2014). There are sites located at high altitudes with dry climate (e.g., in Colorado and Utah), where most of the time Bragg scatter is too weak to be routinely observed.

These three WSR-88D's operational methods use external objects. The first two methods utilize precipitation that makes Z_{DR} calibration "after the fact", i.e., to calibrate Z_{DR}, sufficient amount of data should be collected. The third method (i.e., Bragg scatter) is used in clear air and should be conducted right before a precipitation event and that is not always possible. Stability of the radar system plays a critical role in calibration: a calibrated system should hold constant its parameters for a sufficiently long time or adjust its drift with the built-in equipment. System drifts are monitored on the WSR-88Ds at the end of every volume coverage pattern (VCP). This allows calibrating Z_{DR} with accuracy better than ±0.2 dB on about 60% of systems (Cunningham et al. 2013, R. Lee, personal communication, 2015). No online corrections to the system Z_{DR} from the above mentioned external target methods have been implemented yet. There is a need to continuously verify Z_{DR} calibration with external scatterers. This is not achievable with the above mentioned methods. Ground clutter is observed always and can be tested as a calibration object. In this report, results of studying ground clutter for monitoring Z_{DR} calibration at S frequency band are presented. The following questions are discussed:

- is ground clutter stable enough to be used for monitoring calibration of Z and Z_{DR}? Does Z_{DR} from ground clutter depend on season, wetness of the ground, rain, the wind near the ground and other factors?
- how does Z_{DR} from ground clutter correlate with the system derived Z_{DR}?
- how does Z_{DR} from ground clutter correlate with Z_{DR} obtained from Bragg scatter?

2. Ground clutter as a radar calibration object

The characteristics of radar signals reflected from the ground have been studied for a long time to get information on the types of surfaces, vegetation, the wind near the ground or sea and other environmental features (see a historical overviews in Long 1975 and Billingsley 2002). Dual polarization radar technique has increased the quality of remote sensing of the land and sea and is widely used in SAR radars (e.g., Lee and Pottier 2009). Distributions of the power of reflected signal and their temporal and spatial characteristics have been studied intensively (e.g.,

Billingsley 2002, Kulemin 2003, Lee and Pottier 2009, Curtis 2009) and large amount of data has been obtained at different spectral bands.

The utilization of ground clutter for reflectivity calibration has been studied since 1970s. Rinehart (1978) reported on using reflections from relatively stable point targets (radio towers) to monitor reflectivity calibration. His measurements showed large variations (more than 7 dB) in reflected powers over time. Delrieu et al. (1997) and Pellarin et al. (1999) utilized reflection from mountains to estimate attenuation at X band. Assuming stable reflections from certain mountains, the authors estimated attenuation caused by precipitation located between the radar and mountains. The presented variations in reflectivity from Mount Saint Cyr for dry periods show the day-to-day reflectivity fluctuations of about ±2 dB and ±3 dB for a period of 8 months (Delrieu et al. 1997, their Fig. 3). Vukovic et al. (2015) used ground clutter to monitor reflectivity from a C-band weather radar.

High stability of the system Z_{DR} in X-band radar operated in an urban environment was reported by Borovska and Zrnic (2014). X-band radar of the Bonn University was calibrated on Z_{DR} with vertically looking antenna. Z_{DR} was also measured from ground clutter within distances of 20 km from the radar and in areas with $Z > 50$ dBZ. The median Z and Z_{DR} from ground clutter exhibited high stability during 17 days of the observations: Z_{DR} was within an interval of ±0.12 dB. These authors also presented observations at S band (WSR-88D KOUN) which showed fluctuations in Z_{DR} from ground clutter in an interval of ±0.2 dB over 3.5 days of the observations.

Whereas the cited results are very promise they don't address directly the issues of calibration on the WSR-88D. Therefore we explore signal processing to better select stable ground clutter and collect data in various seasons and under various weather conditions.

3. *Z, Z_{DR}, and Φ_{DP} from ground clutter*

Ground clutter depends on the properties of terrain and the rate of antenna rotation. The maximum spectrum width measured with a S-band phased array radar with a stationary beam is about 0.3 m/s (Curtis, 2009).At shorter wavelengths, the spectrum width is wider (Kulemin 2003). The correlation coefficient drops significantly if the antenna is rotating (Zrnic et al. 2006a). Radar Doppler spectra from the ground are formed by two types of scatterers. The first consist of ground, manmade structures, and big tree trunks all of which are stationary and therefore create a DC component in the Doppler spectra; this component is broadened in a deterministic manner by the antenna motion. The second type of scatterers is slowly moving vegetation, which is responsible for most of the spectrum width. The relative strength of these contributors depends on the type of surface, its wetness, season (foliage), and the surface winds (e.g., Billingsley 2002, Kulemin 2003, Curtis 2009). For calibration purposes, the suppression of the second contribution is desirable because it strongly depends upon environmental conditions.

Ground clutter is very variable spatially: the signal power may change by several dB in adjacent range gates along or across the radial. Strong variations in reflected power may occur in a single range gate at moving antenna from pulse-to-pulse due to changes in the number and types of

reflected elements. Thus, the statistical signal properties of ground clutter depends on the antenna rate and can change widely. For instance, the correlation coefficient ρ_{hv} can be high (> 0.95 as for weather objects) at stationary antenna and drop significantly at moving antenna (e.g., Zrnic et al 2006a).

The polarimetric WSR-88D measures six radar variables: reflectivity Z, Doppler velocity v, spectrum width σ_v, differential reflectivity Z_{DR}, differential phase Φ_{DP}, and copolar correlation coefficient ρ_{hv}. We analyze herein Z, Z_{DR}, Φ_{DP}, and ρ_{hv}, which are calculated from received voltages V_h and V_v in the radar channels with horizontally and vertically polarized waves as,

$$P_h = <V_h^* V_h> - N_h, \ \ P_v = <V_v^* V_v> - N_v, \tag{3.1}$$

$$Z = C_r + 10\log_{10}(P_h), \tag{3.2}$$

$$Z_{dr} = P_h / P_v, \ \ \ \ Z_{DR} = 10\log_{10}(Z_{dr}), \tag{3.3}$$

$$\Phi_{DP} = \arg(<V_h^* V_v>), \tag{3.3}$$

$$\rho_{hv} = |<V_h^* V_v>| / (P_h P_v)^{1/2}, \tag{3.5}$$

where $N_{h,v}$ are the noise power in the channels, C_r is the radar constant, and angular brackets stand for time averaging. In the above equations, noise can be ignored because strong signal from the ground is analyzed in this report.

a. Stationary antenna

The estimates of radar variables are calculated from a given number M of radar samples. Due to temporal signal fluctuations the estimates are characterized by distributions. In case of independent fluctuations such as white noise, the distribution of power estimate $\hat{P}$ is (the circumflex denotes estimation

$$W(\hat{P}) = \frac{M^M \hat{P}^{M-1}}{\Gamma(M) \overline{P}^M} \exp\left(-\frac{M\hat{P}}{\overline{P}}\right) \tag{3.6}$$

with $\overline{P}$ is the mean power and $\Gamma(n)$ the gamma function (e.g., Wallace 1953, Lee and Pottier 2009, section 4.2). Fig. 3.1 demonstrates the closeness of the theoretical distribution (3.6) (the blue line) to the radar data (red dots) collected with KOUN with the transmitter off so that the receiver noise is the contributor. Number of samples $M = 16$ which corresponds to the number in the surveillance scan. The mean power was measured in the internal RVP-901 units. Time interval of data collection was 5 min. The total number of power samples is about 1.5×10^9. One can see that the radar data are in perfect agreement with theory.
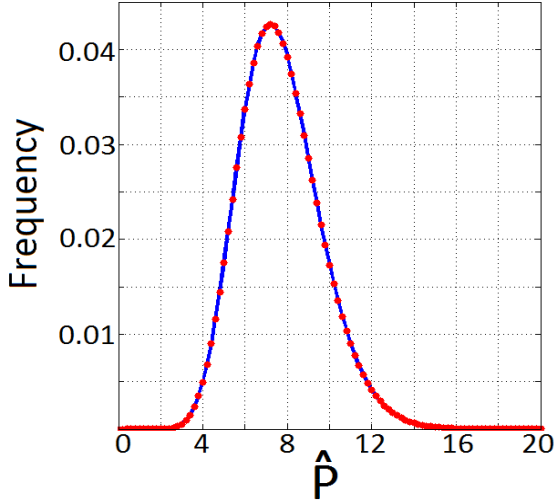
Fig. 3.1. Theoretical distribution eq. (3.6) (the blue line) and radar data (the red dots) collected with RVP-901 with the transmitter off and M =16, $\bar{P}$ = 8 in internal power units. KOUN, May 2, 2015 at 0007 UTC.

Ground clutter returns exhibit narrow Doppler spectra making the number of independent samples lower that the number of samples used in the estimate. The number of independent samples M_i is obtained as (Melnikov and Zrnic 2004)

$$M_i = \frac{M^2}{\displaystyle\sum_{m,n=1}^{M} \exp\{-[(4\pi(n-m)\sigma_v T / \lambda]^2\}} \approx 4MT\,\pi^{1/2}\,\sigma_v/\lambda, \tag{3.7}$$

where σ_v is the spectrum width, T is the pulse repetition time, and λ is the radar wavelength. The approximate in (3.7) is valid and errors are less than 10% if $0.04 \le 4\sigma_v T/\lambda \le 0.60$.

The distribution of the M-sample estimate of differential reflectivity $\hat{Z}_{dr}$ in power units is (Lee and Pottier 2009, section 4.9)

$$W(\hat{Z}_{dr}) = \frac{\Gamma(2M)(1-\rho_{hv}^2)^M(1+\hat{Z}_{dr}/\bar{Z}_{dr})(\hat{Z}_{dr}/\bar{Z}_{dr})^{M-1}}{\Gamma^2(M)[(1+\hat{Z}_{dr}/\bar{Z}_{dr})^2 - 4\rho_{hv}^2\hat{Z}_{dr}/\bar{Z}_{dr}]^{M+0.5}} \tag{3.8}$$

where $\bar{Z}_{dr}$ is the mean. The latter equation is valid for the simultaneous transmission radar mode. Theoretical distributions (3.8) of $\hat{Z}_{dr}/\bar{Z}_{dr}$ are shown in Fig. 3.2 for $M =16$ and $M = 57$; these M are used in the surveillance and Doppler scans in VCP11.
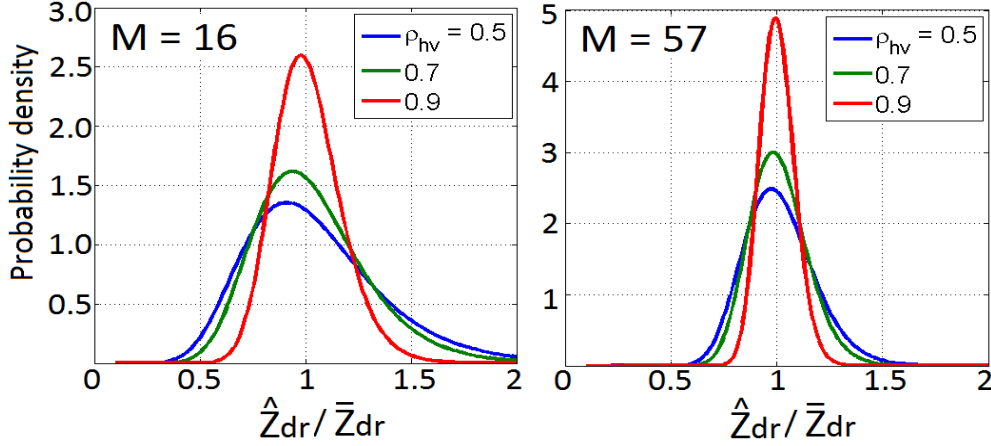
7

Fig. 3.2. Theoretical probability densities for estimates of Z_{dr} in power units for M = 16 (left) and M = 57 (right) for indicated copolar correlation coefficients. M is the number of independent samples.

The distribution of the M-sample $\hat{\Phi}_{DP}$ estimate is (e.g., Middleton 1960, eq. 9.32, Lee and Pottier 2009, section 4.6)

$$W(\hat{\Phi}_{DP}) = \frac{\Gamma(M+0.5)(1-\rho_{hv}^2)^M \beta}{2\pi^{1/2}\Gamma(M)(1-\beta^2)} + \frac{(1-\rho_{hv}^2)^M}{2\pi} \, {}_2F_1(M,1;1/2,\beta^2) \tag{3.9}$$

with $\beta = \rho_{hv}\cos(\hat{\Phi}_{DP} - \overline{\Phi}_{DP})$ and ${}_2F_1$ is the hypergeometric Gauss function. Equation (3.9) is valid for the simultaneous transmission radar mode. The phase Φ_{DP} in (3.9) is strictly due to differential phase on backscattering by ground clutter because we consider clutter without intervening precipitation.

As it was already stated, ground clutter exhibits very narrow spectra if the antenna is stationary. This makes the number of independent samples much smaller than the total number used in the estimates. For instance, at $\sigma_v = 0.1$ m s^{-1} and PRF = 320 Hz (the surveillance WSR-88D's scan), $Mi = 0.18$ at $M = 16$, i.e., the number of independent samples is about two orders of magnitude less than the total number of samples. For the Doppler WSR-88D's scan ($M = 57$), $Mi = 0.40$. Such a small Mi allows using eqs. (3.6), (3.8), and (3.9) in simplified forms for $M = 1$:

$$W(\hat{P}) = \frac{1}{\overline{P}}\exp\left(-\frac{\hat{P}}{\overline{P}}\right), \tag{3.10}$$

$$W(\hat{Z}_{dr}) = \frac{(1-\rho_{hv}^2)(1+\hat{Z}_{dr}/\overline{Z}_{dr})}{[(1+\hat{Z}_{dr}/\overline{Z}_{dr})^2 - 4\rho_{hv}^2\hat{Z}_{dr}/\overline{Z}_{dr}]^{3/2}}, \tag{3.11}$$

8

$$W(\hat{\Phi}_{DP}) = \frac{1-\rho_{hv}^2}{2\pi(1-\beta^2)}\left[1+\beta\frac{\pi/2+\sin^{-1}\beta}{(1-\beta^2)^{1/2}}\right]. \tag{3.12}$$

To verify the latter equations, radar data at stationary antenna have been collected with KOUN. Fig. 3.3 shows an example of radial profiles of SNR and Doppler velocities (left panel) at an azimuth of 220° and an elevation of 0.5^o (the lowest elevation in the WSR-88Ds). In the right panel, SNR_h and Z_{DR} for the same radial are depicted. One can see that the Doppler velocity is almost zero within range of 27 km and slightly increases beyond that distance because of contribution from biota. Biota is recognized from high Z_{DR} at those distances (the right panel). It is also seen that SNR is larger than 40 dB (the SNR threshold in our study) within distances of 27 km from the radar. At a distance of several kilometers from the radar, the SNR > 50 dB.
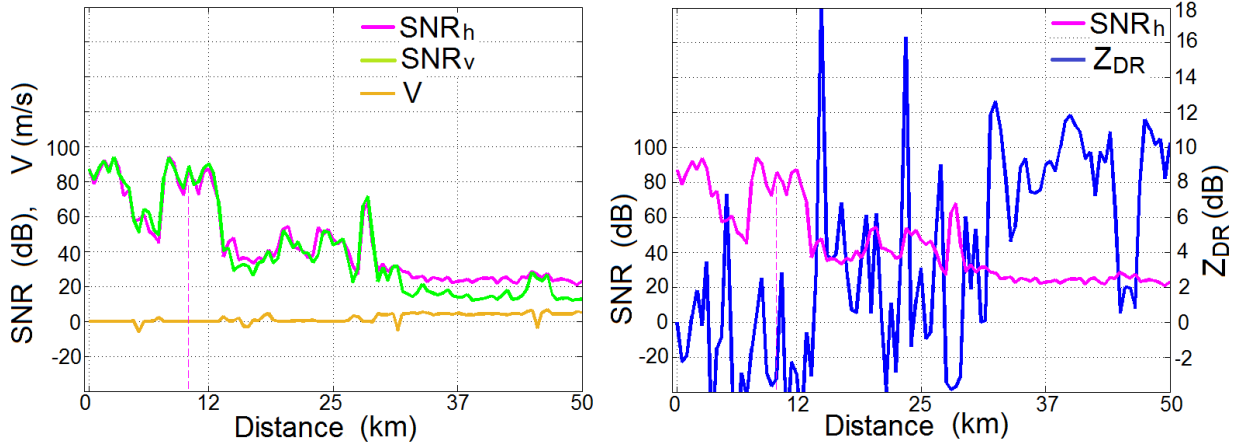

Fig. 3.3. Radial profiles of (left) SNR and Doppler velocity and (right) SNR_h and Z_{DR}. KOUN 06/02/2015 at 0041 UTC, azimuth 220° elevation 0.48^o, long pulse mode.

Distributions of SNR, Z_{DR}, and Φ_{DP} estimates from a single range gate at the distance of 10 km are shown in Fig. 3.4 with the blue lines ($M = 64$, the data were collected for about 5 min). This range gate is shown in Fig. 3.3 with the magenta dashed vertical lines. Figs. 3.4a,b show the distributions of SNR in the two polarimetric channels. It is seen that the red lines, which correspond to the theoretical distribution with $M = 1$, i.e., eq. (3.10), approximates the radar data well (distribution W_1 in the figure). This means that radar data are strongly correlated and the number of independent samples is close to 1. The green lines in the panels present SNR distributions for $M = 2$ (distribution W_2 in the figure). We can conclude that the distribution for M = 1 is closer to the data than that for M = 2.

Distribution of Φ_{DP} is shown in panel (c). The red line is the distribution (3.12) for $M = 1$ and $\rho_{hv} = 0.5$. It is seen that one-pulse distribution approximates radar data well. One can see a well pronounced maximum of the distribution that corresponds to the system differential phase $\psi_{sys} = \psi_t + \psi_r$ with $\psi_{t,r}$ being the system differential phases in transmit and receive (Zrnic et al. 2006a). The theoretical distribution of Z_{dr} is shown in panel (d) for $M = 1$ and $\rho_{hv} = 0.5$, i.e. eq. (3.11), with the red line. A general conclusion is that the theoretical distribution for $M = 1$

9

approximate well the radar data from ground clutter collected from a single range gate and with the stationary antenna.
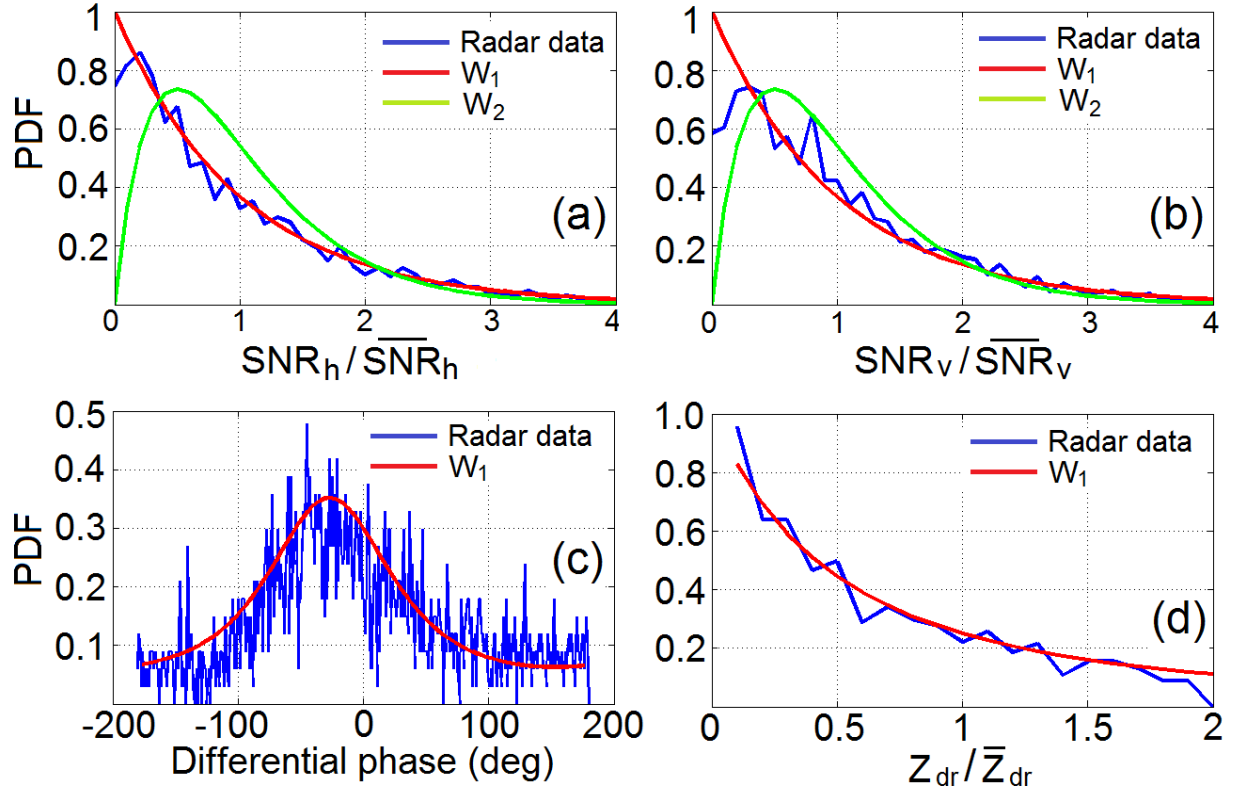

Fig. 3.4. Distributions of (a, b) the powers in horizontal and vertical channels, (c) differential phase, and (d) Z_{dr}. KOUN, 06/02/2015 at 0041 UTC, azimuth 220° elevation 0.48^o, R = 10 km, long pulse mode (the blue curves). W_1 and W_2 are theoretical distributions (see the text).

b. Rotating antenna

The above results can be applied to a rotating antenna with caution because ground clutter is highly variable spatially. As the antenna is rotating, the number of reflecting elements in the radar resolution volume changes; this decreases the effective copolar correlation coefficient and increases the number of independent samples. But at the same time, the signal may lose stationarity and its mean characteristics may vary. One of the most important questions in calibration is feasibility of using ground clutter during regular data collection. So the data from standard VCPs are used in the following discussion.

An example of six radar variables collected with KOUN in "clear air" is shown in Fig. 3.5 to the range of 50 km where the echo from ground clutter is mainly located. The SNR field contains values from 10 to 90 dB. The velocity field shows predominant positive values in the north part of the field and mainly negative values in the south part. This shows that radar captured signals from insects/birds that were flying to the north. High Z_{DR} values at the edges of the Z_{DR} field

confirm this conclusion. The spectrum width field has small values in areas with strong signals and much larger values in areas with atmospheric biota. The differential phase field has predominant values in an interval of $70 - 120°$ (brown and yellow colors). The vast majority of ρ_{hv} values is lower than 0.9 however one can see high values (> 0.9) in some areas filled with biota.
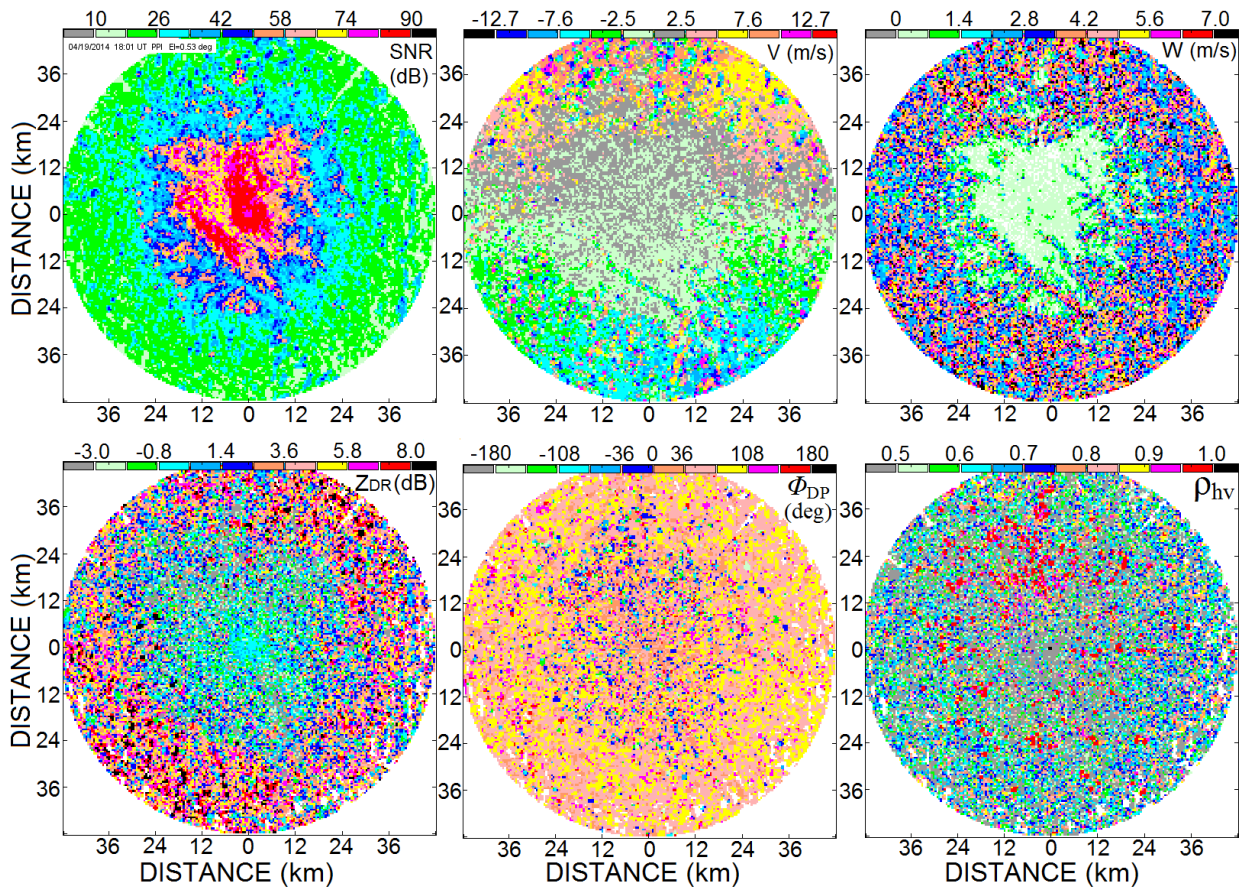

Fig. 3.5. Six radar variables collected with KOUN on April 19, 2014 at 1801 UTC in "clear air" and shown to a distance of 50 km.

To select ground clutter for this study, echoes from biota and moving ground objects (for instance, vehicles) should be filtered out. To do so, the following constraints were applied to radar data.

a. Range of observation is within the interval from 2 to 30 km, where most of ground clutter is located on this site. For other radar sites, areas with strong ground clutter can be different and should be chosen using strongest reflected powers.

b. SNR threshold was set at 40 dB in both polarimetric channels. This filters out a great deal of atmospheric biota.

c. Parts of the Doppler spectra from an interval ±0.5 m s^{-1} are processed to select echoes from stationary ground targets. Filtering out signals with spectral components beyond this threshold throws away the signal contributions from moving clutter (tree/bush branches, moving vehicles, and flying birds) and also rejects signals leaking from strong stationary clutter (i.e., spectral leakage).

To illustrate the latter constraint, Doppler spectra from a range gate shown in Fig. 3.4 are displayed in Fig. 3.6 for $M = 16$ and 64 (PRF = 320 Hz). A strong spectral leakage is seen in the spectra. These spectral skirts can have contributions from moving ground targets (tree branches, vehicles, and birds) and illustrate the reason we censored these. To suppress the spectral skirts, the spectral part in the interval ±0.5 m s^{-1} is selected for further analysis. This spectral interval is located between the brown vertical lines in Fig. 3.6. After suppressing spectral skirts, the selected spectrum is converted to I/Q signal components and all signal characteristics are calculated in time domain according to (3.1) - (3.5). For M =16, only one spectral component, i.e., DC, is left in the spectra (Fig. 3.6a), for M=64, three central lines are left in the spectra.
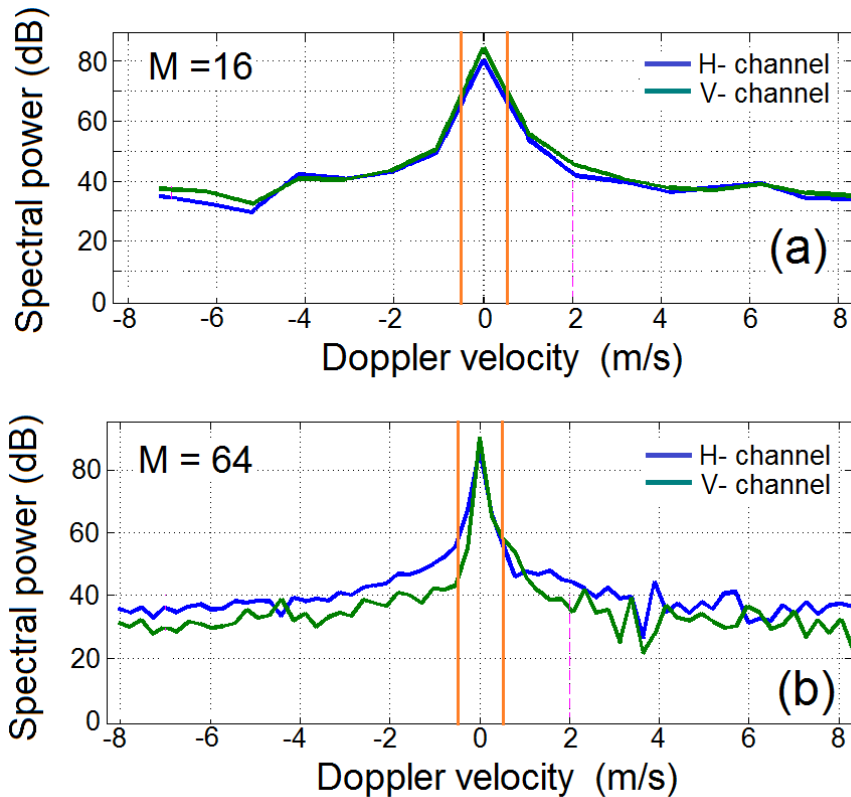

Fig. 3.6. Doppler spectra in the two polarimetric channels for the range gate shown in Fig. 3.3 with the vertical magenta dashed line. The number of samples is (a) M =16 and (b) $M = 64$. The two brown vertical lines are drawn at velocities ±0.5 m s^{-1}.

There are two "clear air" VCPs in the WSR-88Ds: VCP31 and VCP32. The parameters of these VCPs are in Table 1. VCP31 uses the long radar pulse (4.5 μs) and VCP32 operates with the short radar pulse (1.5 μs). The lowest antenna elevation for both VCPs is 0.5°.

Table 1. Parameters of VCP 31 and 32.

VCP	Lowest elevation, deg	Scanning mode	Pulse width	PRF, Hz	Nyquist velocity, m/s	Number of samples	Number of spectral lines left in the spectrum
31	0.5	Surveillance	Long	326	9.0	64	3
		Doppler	Long	452	12.4	87	3
32	0.5	Surveillance	Short	326	9.0	66	3
		Doppler	Short	1027	28.2	226	5
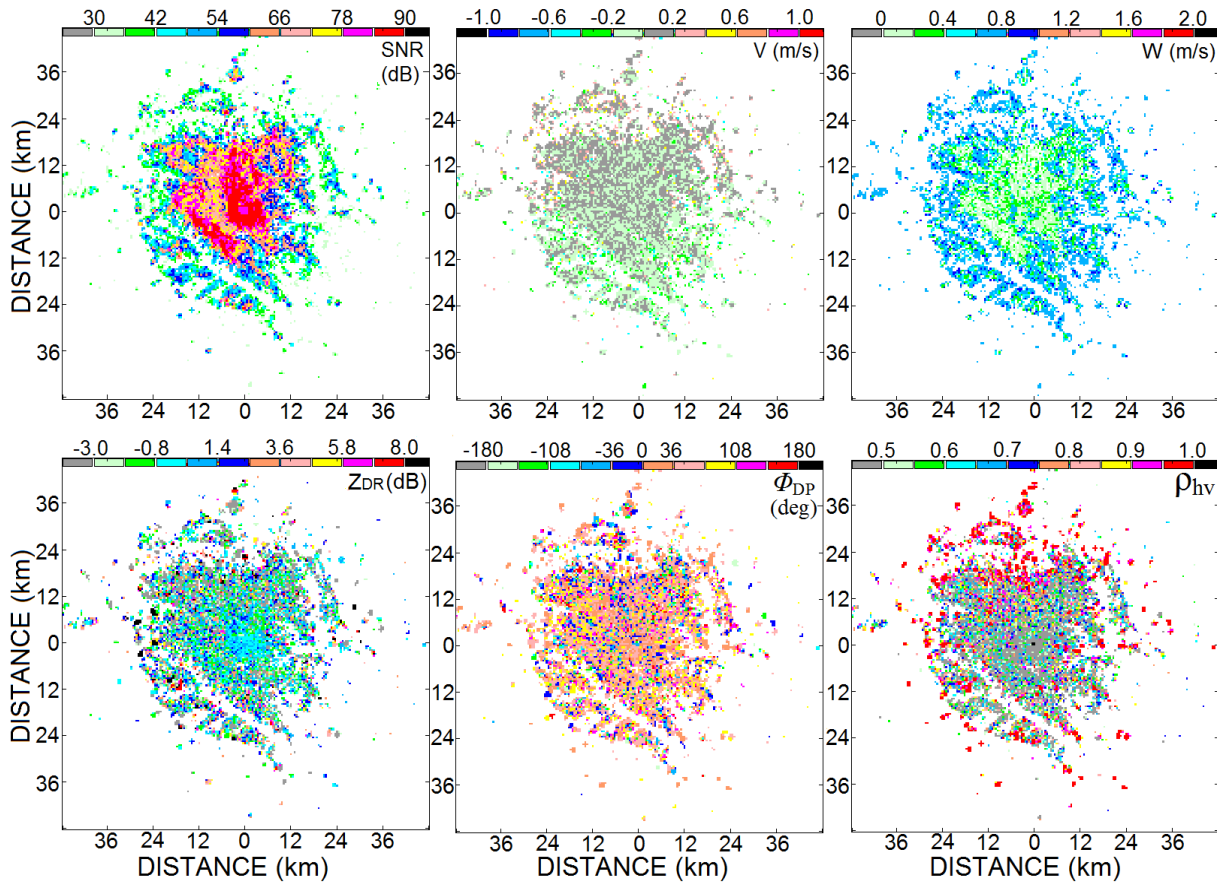
Fig. 3.7. Fields of six radar moments obtained using constraints a-c above with the SNR threshold of 30 dB.

13

An example of clutter echo with SNR threshold of 40 dB is in Fig. 3.7. The data have been obtained for the spectra within the interval ±0.5 m s^{-1}. One can see that a big portion of biota echoes has been removed from the images. The spectrum width field has values less than 1 m s^{-1} now (compare with Fig. 3.5).

Distributions of SNR$_h$, Φ_{DP}, and Z$_{DR}$ obtained with the three constraints at SNR $\geq$ 40 dB are shown in Fig. 3.8. The Φ_{DP} distribution has a similar form as in Fig. 3.4 with the maximum at the system differential phase.
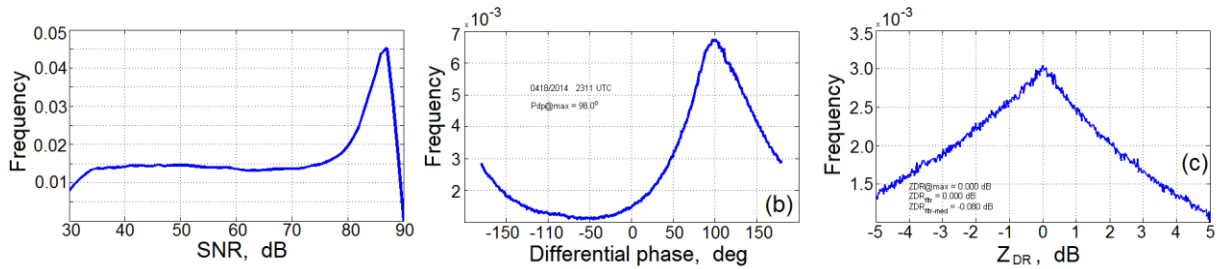
Fig. 3.8. Distributions of SNR (a), Differential phase (b), and ZDR for data collected on April 19, 2014 from 0000 to 0200 UTC. The total number of data is 2.17x10^6.

4. Studied parameters of the distributions

The right panel in Figs. 3.8 exhibits a well pronounced peak of Z$_{DR}$ distribution at a value close to zero. The system Z$_{DR}$ in KOUN at that time was 0.25 dB, i.e., also close to 0 dB. One of the main goals of this study is obtaining stability of the distributions of Z$_{DR}$ from ground clutter. To assess this stability as well as stability of the SNR and Φ_{DP} few parameters of their distributions were studied. These are

   For Z$_{DR}$:

   a. The mean Z$_{DR}$ value in the interval -5 to 5 dB (ZDR$_{mean}$),
   b. The median Z$_{DR}$ value in the interval -5 to 5 dB (ZDR$_{median}$),
   c. Z$_{DR}$ value at the maximum of distribution (ZDR$_{max}$),
   d. Z$_{DR}$ value at the maximum of filtered distribution (ZDR$_{fltr1}$) using the Golay filter,
   e. Z$_{DR}$ value at the maximum of filtered distribution (ZDR$_{fltr2}$) using the median filter.

   For SNR:
   f. The mean SNR in the polarimetric channels (SNRmean).
   g. The median SNR in the polarimetric channels (SNRmedian).
   h. SNR at the maximum of its distribution (SNRmax).

   For Φ_{DP}:
   i. Differential phase at the maximum of its distribution (Φ_{DPmax}).

The algorithm of data processing consisted of the following steps

14

For Z_{DR}:

- Select data with SNR $\geq$40 dB in both channels.
- From obtained data, select range gates that contain Z_{DR} in interval -5 to 5 dB.
- Compute Z_{DR} in selected range gates ($ZDR_{selected}$) and obtain $ZDRmean = <ZDR_{selected}>$.
- Compute $ZDRmedian = median(ZDR_{selected})$
- Obtain Z_{DR} at the maximum of its distribution (ZDR_{max})
- Obtain distribution of the $ZDR_{selected}$ values. Filter the distribution with the Golay filter and obtain Z_{DR} at the maximum of filtered distribution (ZDR_{fltr1}).
- Apply the median filter to the distribution and obtain Z_{DR} at the maximum of filtered distribution (ZDR_{fltr2}).

The calculations of ZDR_{fltr1} and ZDR_{fltr2} are demonstrated in Fig. 4.1. A distribution obtained with the Golay filter with scale = 19 is shown in the left panel of the figure with the red curve. The maximum of this distribution lies at 0.00 dB, i.e., $ZDR_{fltr1} = 0.00$ dB. The distribution of radar data are also filtered with the median filter with scale = 19 (the brown curve in the right panel of Fig. 4.1). The maximum of this distribution lies at -0.08 dB, i.e., $ZDR_{fltr2} = -0.08$ dB. The maximum of the unfiltered data lies at 0.00 dB, i.e., $ZDR_{max}= 0.00$ dB
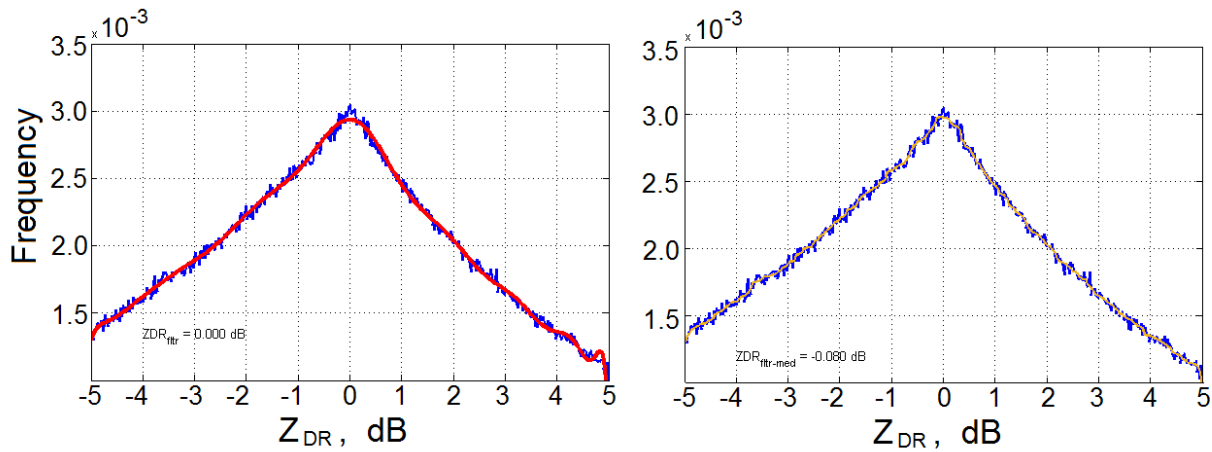

Fig. 4.1. Distribution of Z_{DR} data (the blue line) and approximations of the distribution with the Golay (left panel, the red line) and median (right panel, the brown line) filters. The maximum of the Golay filtered distribution is 0.00 dB, the maximum of the median filtered distribution is -0.08 dB. WSR-88D KOUN, April 19, 2014 from 0000 to 0200 UTC.

For SNR:

- Select data with SNR $\geq$40 dB in both channels.
- From obtained data, select range gates that contain Z_{DR} in interval -5 to 5 dB.
- Compute SNR in selected range gates and obtain $SNRH_{mean} = <SNRH_{selected}>$ and $SNRV_{mean} = <SNRV_{selected}>$ in the two polarimetric channels.
- Compute $SNRH_{median} = median(SNRH_{selected})$ and $SNRV_{median} = median(SNRV_{selected})$
- Obtain SNR at the maximum of its distribution ($SNRH_{max}$ and $SNRV_{max}$).

An example of SNR distribution is shown in Fig. 4.2. The mean SNR in the channels are calculated from data selected in the Z_{DR} interval of ±5 dB. The maximum of distributions is at 86.7 dB (the horizontal channel) and shown in the figure with the vertical red line.
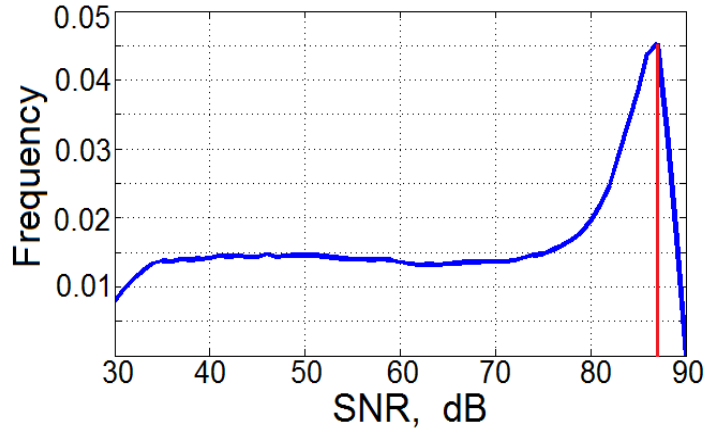

Fig. 4.2. Distribution of SNR in the horizontal radar channel with the maximum at 86.7 dB. WSR-88D KOUN, April 19, 2014 from 0000 to 0200 UTC.

For Φ_{DP}:

-   Select data with SNR ≥40 dB in both channels.
-   From these data, select range gates that contain Z_{DR} in interval -5 to 5 dB.
-   Compute Φ_{DP} in the selected range gates and obtain a distribution/histogram. Obtain Φ_{DP} at the maximum of its distribution (Φ_{DPmax}).
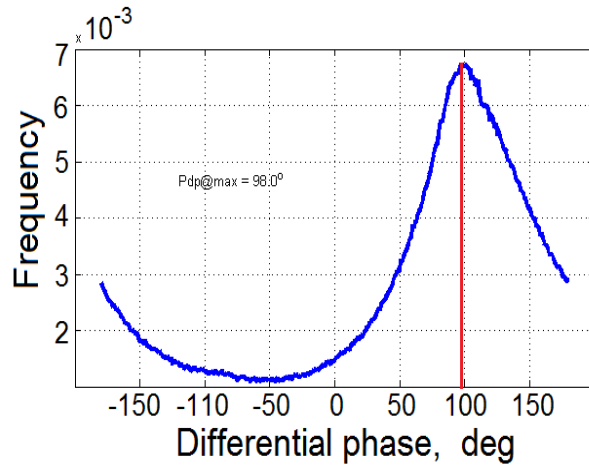

Fig. 4.3. Distribution of Φ_{DP}; the maximum is at Φ_{DPmax} = 98°. WSR-88D KOUN, April 19, 2014 from 0000 to 0200 UTC.

The maximum of distribution is at 98° (Fig. 4.3) and its location is indicated with the vertical red line.

Fig. 4.4 presents time series of Z_{DR} values from ground clutter obtained using a different algorithms. The blue line represents Z_{DR} at the locations of the maximum of Z_{DR} distributions as one shown in Fig. 4.1 with the blue line. The green line in Fig. 4.4 is Z_{DR} at the maximum of the distributions smoothed with the Golay filter. The red line is Z_{DR} at the maximum of Z_{DR} distributions smoothed with the median filter. It is seen that the blue line exhibits larger variations compared with two other lines. The Golay filtered data exhibits minimal variations so this algorithm is used to estimate Z_{DR} from the ground.
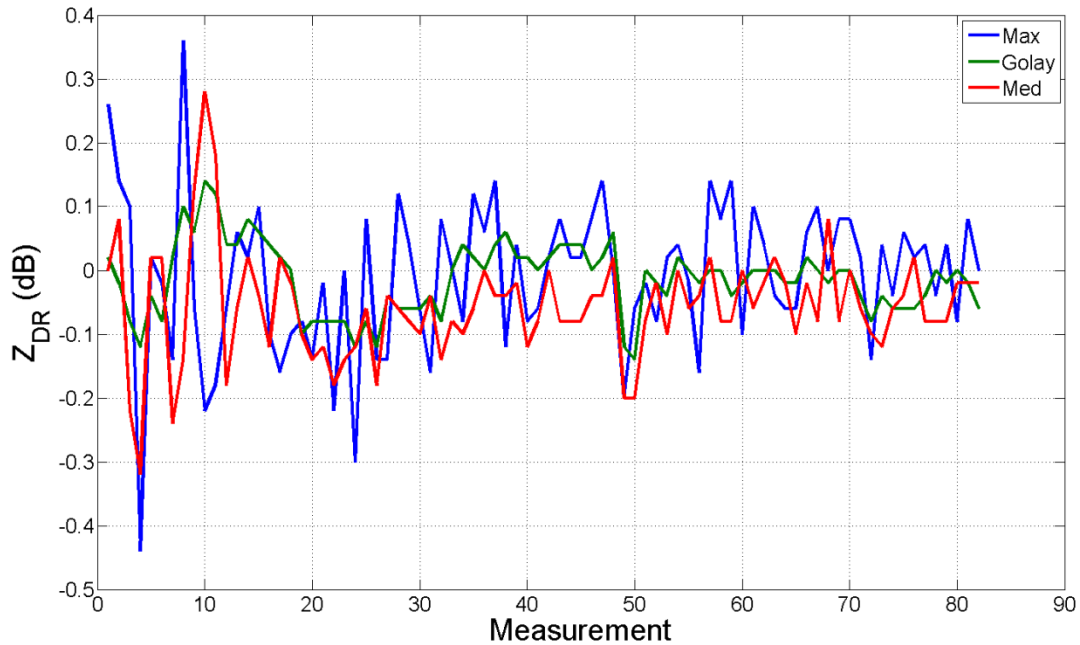

Fig. 4.4. Time series of Z_{DR} from ground clutter from March to September, 2014. WSR-88D KOUN, RVP8 processor. The blue line is Z_{DR} at maxima of the distributions. The green line is Z_{DR} filtered by the Golay filter. The red line is Z_{DR} filtered by the median filter.

5. The baseline Z_{DR} calibration procedures in the WSR-88D

The WSR-88Ds measures the system Z_{DR} at the end of a VCP, and applies this bias to the data in the next VCP. This measurement is called the baseline calibration. Two main parameters are measured during this calibration: biases of the receiver (RCB) and transmitter (TXB). Bias of the antenna and surrounding waveguides are obtained from solar measurements (SMB) that are done every 8 hours if the sun is available and there is no precipitation (Zrnic et al. 2006b, Melnikov et al. 2013, Ice et al. 2014).

$$ZDRsys = 2* SMB + RCB + TXB. \quad\quad\quad (5.1)$$

17

The antenna bias can be considered constant over time because this system part does not contain active elements. On KOUN, it is -0.14 dB. The receiver and transmitter biases change over time because their hardware contains active components with time-varying gains. These variations should be monitored by the system and accounted for during weather observations.
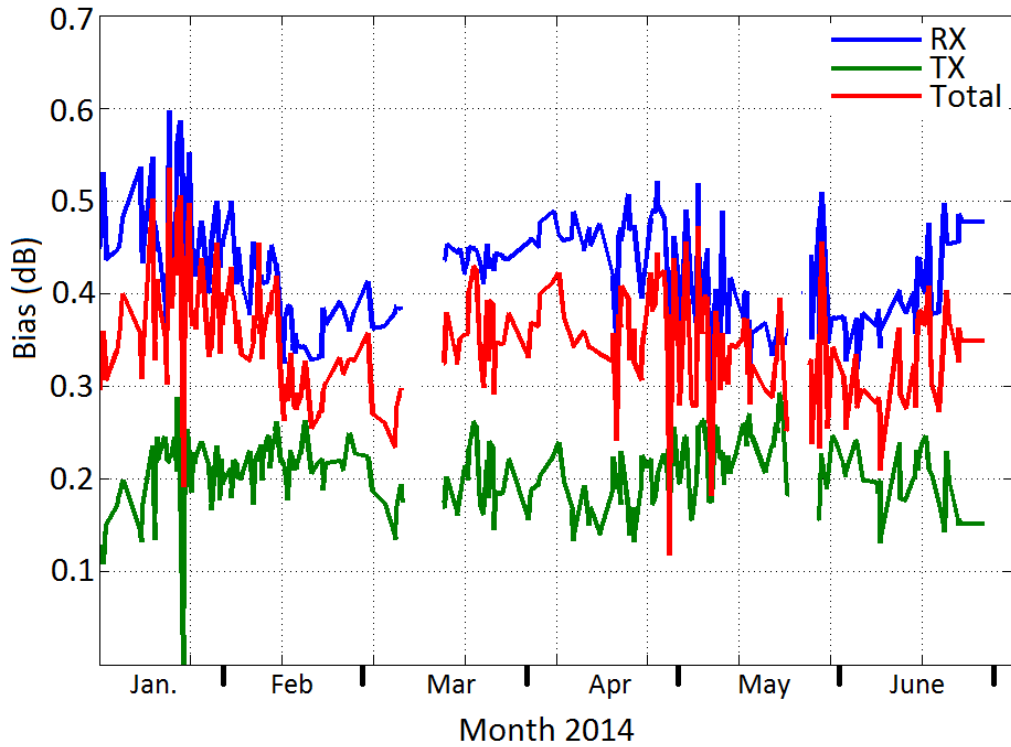

Fig. 5.1. The receiver (RX, blue line), transmitter (TX, green line), and total (red line) system Z_{DR} biases in KOUN from January to June 2014. RVP8 processor.

Fig. 5.1 shows time series of the system Z_{DR} biases from the transmitter (RX), receiver (TX), and total one collected on the KOUN with the RVP8 processor. The contributions in the system Z_{DR} bias are given by eq. (5.1). One can see in Fig. 5.1 the variations of the transmitter Z_{DR} bias are smaller than those from the receiver. So the variations in the total Z_{DR} bias come mostly from the instability of the receiver.

The data in Fig. 5.1 were collected with the processor RVP8. In the beginning of 2015, the RDA processor on KOUN was replaced with a RVP9. The system biases obtained on the RVP9 are shown in Fig. 5.2 for June 2015. Again, one can see that the variations in the system bias are mostly determined by variations of the receiver gain. The brown line in Fig. 5.2 presents the temperature inside the temperature controlled enclosure of the Antenna Mounted Electronics (AME). Diurnal temperature variations of 0.5^{o}C are apparent. These variations cause variations in the receiver bias and correspondingly in the total bias. The drops in the AME temperature lead to the increases in the system bias. The transmit bias does not show any dependence on the AME

temperature although some measurement hardware is located in the AME box. The amplitude of the temperature variations in the total Z_{DR} bias is about 0.2 dB. This bias is applied in the calculations of Z_{DR}, so the system compensates for this hardware instability. Similar behavior of the system was observed in July-October 2015.
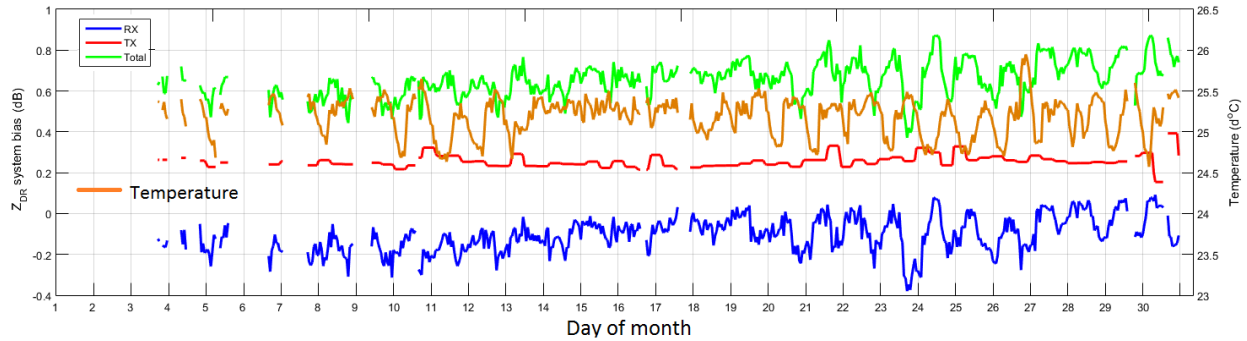

Fig. 5.2. The receiver (RX, blue line), transmitter (TX, red line), and total (green line) system Z_{DR} biases in KOUN in June 2015 measured on the RVP9 processor. The temperature (^oC) in the AME is shown with the brown line.

6. Feasibility of reflectivity monitoring

Radar reflectivity Z is calculated from signals in the horizontal radar channel so stability of Z depends upon stability of the transmitter and receiver in this channel. The system should be capable of monitoring variations in the transmit power and receiver gain. For that the signal-to-noise ratio (SNR_h, the horizontal channel) from ground clutter could be used and therefore its stability is analyzed. The SNR is determined as a ratio of the returned signal power to noise power. The SNR from ground clutter is caused by stationary (e.g., buildings) and moving (e.g., tree branches and vehicles) scatterers. Our initial observations with KOUN suggest that SNR_h depends also on the presence of insects and birds in the atmosphere, wind near the ground and wetness of the ground i.e., it is not stable within 1 dB that is needed to monitor system stability. Therefore some censoring of clutter signal is needed to improve its stability. For that reason suitability of few spectral lines near zero Doppler are studied and the term SNR_h hereafter refers to the SNR of signals with the narrow spectrum. Signal processing to obtain this spectrum has been described in section 4b.

Time series of the mean SNR_h is shown in Fig. 6.1. This mean SNR_h has been calculated by using return power from ground clutter collected at the lowest antenna elevation during one hour. The gaps in the curve correspond to periods when data were not available.

The brown line (Fig. 6.1) represents the pulse width: the upper part of the line corresponds to the long pulse and the lower part corresponds to the short pulse. As expected, the mean reflected power depends on the width of the radar pulse. One can see that the mean SNR_h for the short pulse is about 3 to 4 dB lower than that for the long pulse. If homogenous scatterers like rain fill the resolution volume, this difference should be 9 dB; because ground clutter is highly variable in range and is not exactly volumetric scatterers this difference is smaller.
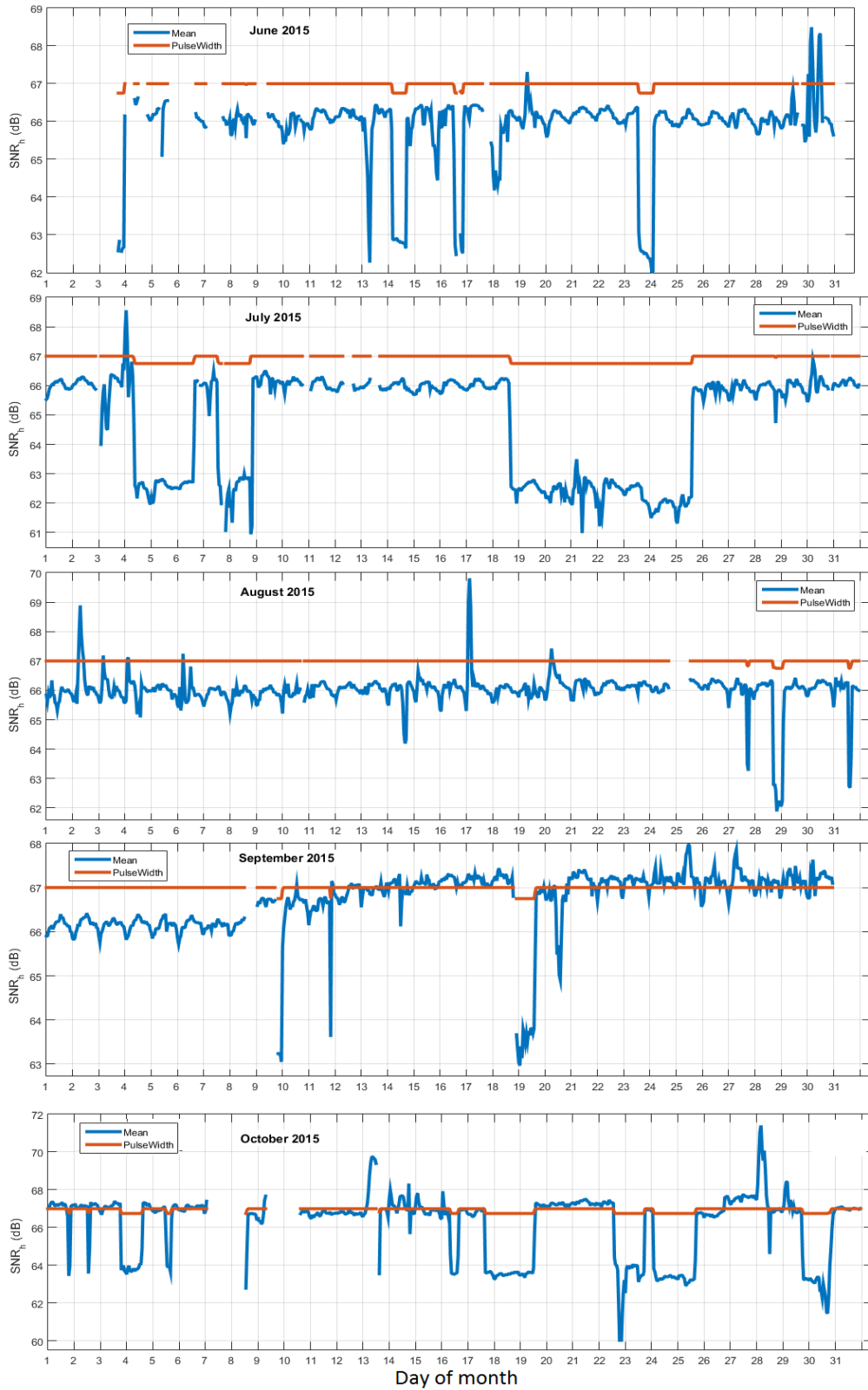
19

Fig. 6.1. Mean SNR$_h$ from ground clutter (the blue line) from June to October 2015. WSR-88D KOUN. The brown line represents the pulse width.

One can see that the mean SNR_h increased over time from 66.2 dB (for the long pulse) in June 2015 to 67.1 dB in September and October 2015. This could be due to a time change in vegetation, but one can expect some drop in the reflected power from more dry vegetation in October than in June. So this SNR_h growth is likely due to a system drift.

One can also see variations in SNR_h at a particular pulse width. For instance, a 4-dB drop in SNR_h on 13 June 2015 at about 6 UTC, 2.5-dB jumps on 30 June 2015, 2.5-dB oscillations on 19-25 July 2015 in the short pulse mode, 4-dB jump on 17 August 2015, and others.
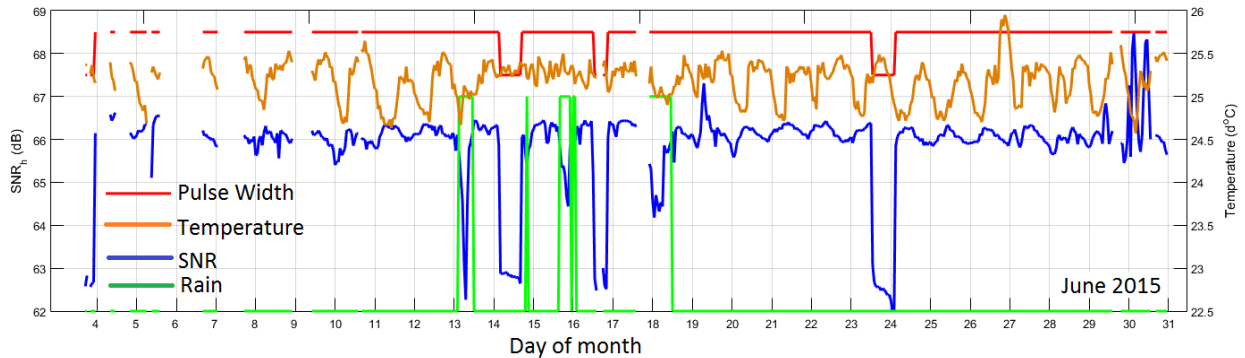

Fig. 6.2. Mean SNR_h from ground clutter (the blue line), the pulse width (red line), rain (green line), and AME temperature (brown line) in June 2015. WSR-88D KOUN.

Occurrences of rain events are indicated in Fig. 6.2 with the green line. It is seen that the rain times correlate with the drops of SNR_h. It is hard to imagine that rain in the vicinity of radar decreases reflections from the ground so the decreases are due to the effects of water on the radome during rain. This can be recognized and can be used to correct the attenuation by wet radomes. The increases of SNR_h on 19 and 30 June 2015 (Fig. 6.2) are due to variations in radar parameters and should be monitored by the system. Fig. 6.3 shows the transmit powers measured by the KOUN's system hardware on 19 and 30 June 2015. One can see a drop in the horizontal power at about 06 UTC on 19 June 2015 whereas the SNR from ground clutter increases at that time. The gain of the H-receiver (not shown in the figure) did not change according to the KOUN's parameter log. So the increase of SNR from ground clutter on that day was not compensated by the system. Similar situation was observed on 30 June 2015. So SNR from the ground can be used to monitor short term system gain changes. We do not know if such short term variations are due to changes in the overall system gain or the measurements process or both. Further analysis in needed to resolve this issue.

Variations in SNR_h from ground clutter due to the AME temperature are of 0.5 dB, which is within tolerable interval. The KOUN's data show that the system can be stable over time intervals of several hours to several days. So SNR_h from ground clutter can be used to monitor stability of reflectivity measurements.
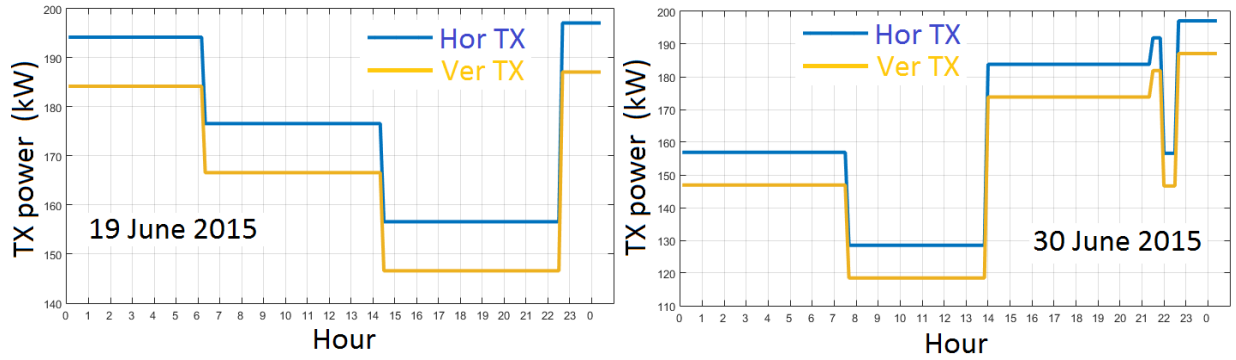
Fig. 6.3. The transmit powers in the horizontal (the blue line) and vertical (the light brown line) channels measured by the system on 19 and 30 June 2015. WSR-88D KOUN.

7. Feasibility of Z_{DR} monitoring

The signal with the narrow spectra has been used to monitor the stability of Z_{DR} values measured in ground clutter. A time series of the measurements from June to October 2015 is presented in Fig. 7.1. Strong Z_{DR} peaks in the figure are observed during rain events on the KOUN site. It was shown in the previous section that rain decreases the mean SNR_h from ground clutter. Fig. 7.2 shows SNR_h and SNR_v from ground clutter on 13 June 2015. It is seen that both SNRs experienced a drop but the drop in SNR_v is larger than that in SNR_h at rain and become about equal before and after rain. This means that rain attenuates radar signals in both channels, but attenuation in the vertical channel is stronger and that leads to a positive jump of Z_{DR}. There is correlation between rain rate and SNR_h and SNR_v from the ground: signal attenuation in the channels increases with the increasing rain rate. Compare, for instance Fig. 7.2 and the lower panel in Fig. 7.3. But we do not see strong (if any) correlation between the Z_{DR} jumps and rain rates.

Positive jump in Z_{DR} in rain could have a contribution from ground clutter, i.e., reflections from the ground could vary during rain due to wet ground objects. To verify this, Z_{DR} from ground clutter can be measured at times when rain is observed at ranges closer than 50 km but is not present at the radar site. The NORM Mesonet station is located about 200 m to the west from KOUN so rain on the station can be considered as rain on KOUN site as well. The problem with this is that the Mesonet stations measure not rain rates but rain accumulations every 5 min, so the instantaneous rain rate is not available. The second issue is that radar data from the lowest elevation, where parameters of ground clutter are measured, are updated every 9 min in VCPs 31 and 32. So a time correspondence of the Mesonet and radar data is not precise. Figs. 7.3 – 7.9 present Z_{DR} from ground clutter averaged over one antenna sweep and the 5-min averaged rain rate from the NORM Mesonet station. Fig. 7.3 shows weak correlation between Z_{DR} and the averaged rain rate: the strong rain rate maximum at about 0645 UTC does not correspond to a strong maximum in Z_{DR}; values of Z_{DR} are high from 0400 to 0830 UTC. Rain on the site began at about 0330 UTC.
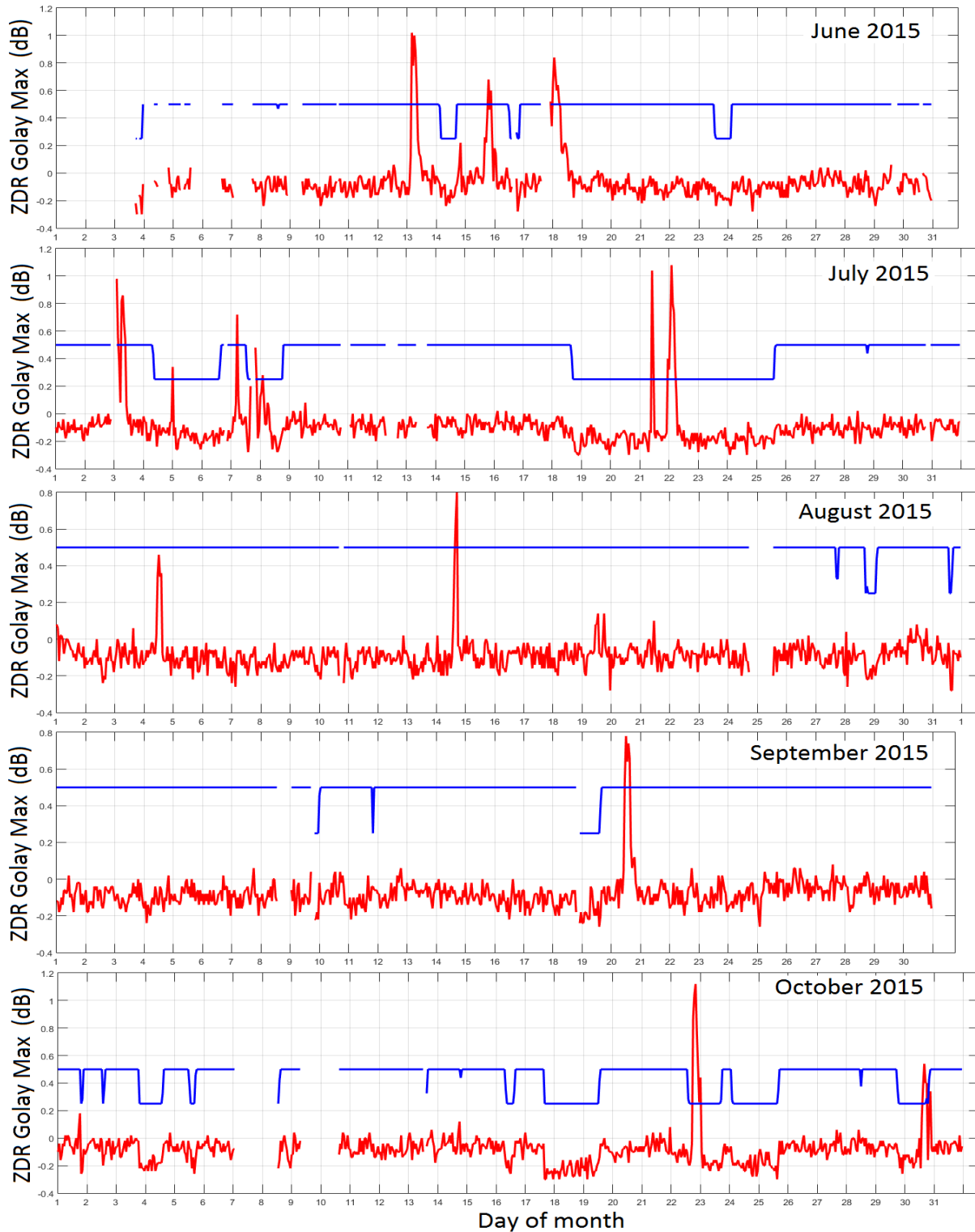
Fig. 7.1. Time series of the system Z_{DR} (the red lines) calculated using the Golay filter. The blue line represents the pulse width: values of 0.5 and 0.25 correspond to the long and short pulses. The curves brake at times when data are not available. WSR-88D KOUN time is UTC.

Fig. 7.4 shows correlation between the rain rate and Z_{DR} at 0330 UTC and 0700-0800 UTC but Z_{DR} does not change in rain between 2100 and 2200 UTC. Fig. 7.5 exhibits a strong change in Z_{DR} at about 0600 UTC at small rain rates. This figure also shows noticeable increase in Z_{DR} before the rain on the site that indicates some rain influence on reflection from the ground. A noticeable increase in Z_{DR} is visible at 1630 UTC (Fig. 7.5) whereas rain on the site began at 1705 UTC. So rain affects Z_{DR} from the ground at that time. No such conclusion can be made from Fig. 7.6 at about 0940 UTC, i.e., Z_{DR} changes at the time of rain on the site not before. Rain on the site at about 0200 UTC did not change Z_{DR} at all. Some Z_{DR} growths before rain on the site are seen in Fig. 7.8 at 1100 UTC and in Fig. 7.9 at 1745 UTC. On the other hand, in Fig. 7.7, the jump in Z_{DR} correlates well with the beginning and ending of rain. Thus there is evidence of some influence of rain on Z_{DR} from the ground therefore to monitor Z_{DR} using ground clutter, such measurements should be taken in the absence of rain over the clutter area (here closer than about 30 km of the radar). Further examination of the effects of rain on the Z_{DR} from clutter very close to the radar remains to be made.
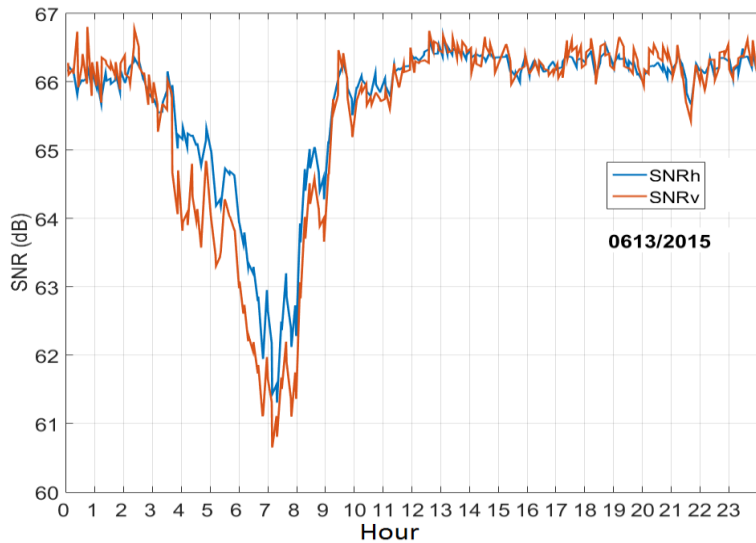

Fig. 7.2. SNR$_h$ and SNR$_v$ from ground clutter on 13 June 2015. Rain on the radar site occurred from about 0340 to 1145 UTC. See rain rates shown in Fig. 7.3.

In dry days, the stability of the mean Z_{DR} from the ground is mainly within ±0.1 dB (Fig. 7.1) and can be used to monitor system Z_{DR}. Note a significant difference in variations of Z_{DR} in Fig. 7.1 and Figs. 7.2-7.9: this is due to averaging over 1 hour of data in Fig. 7.1.
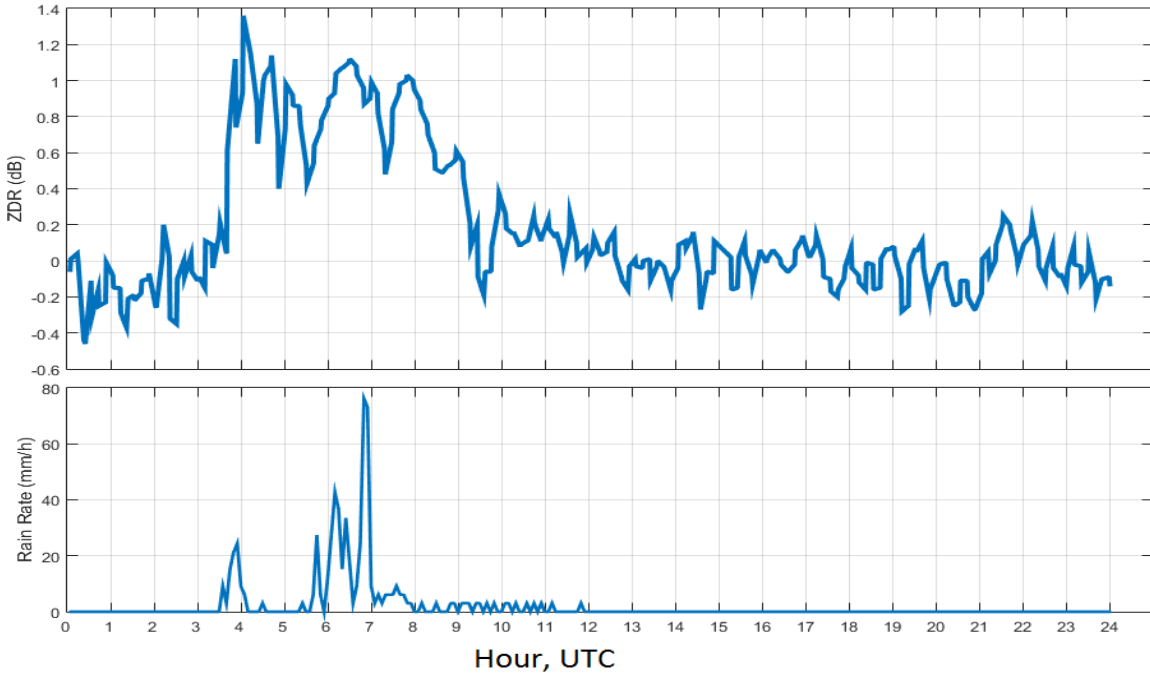
Fig. 7.3. (top): Z_{DR} at the distribution maximum obtained with the Golay filter on 13 June 2015. (bottom): Rain rate measured at the Oklahoma Mesonet station NORM on the same day.
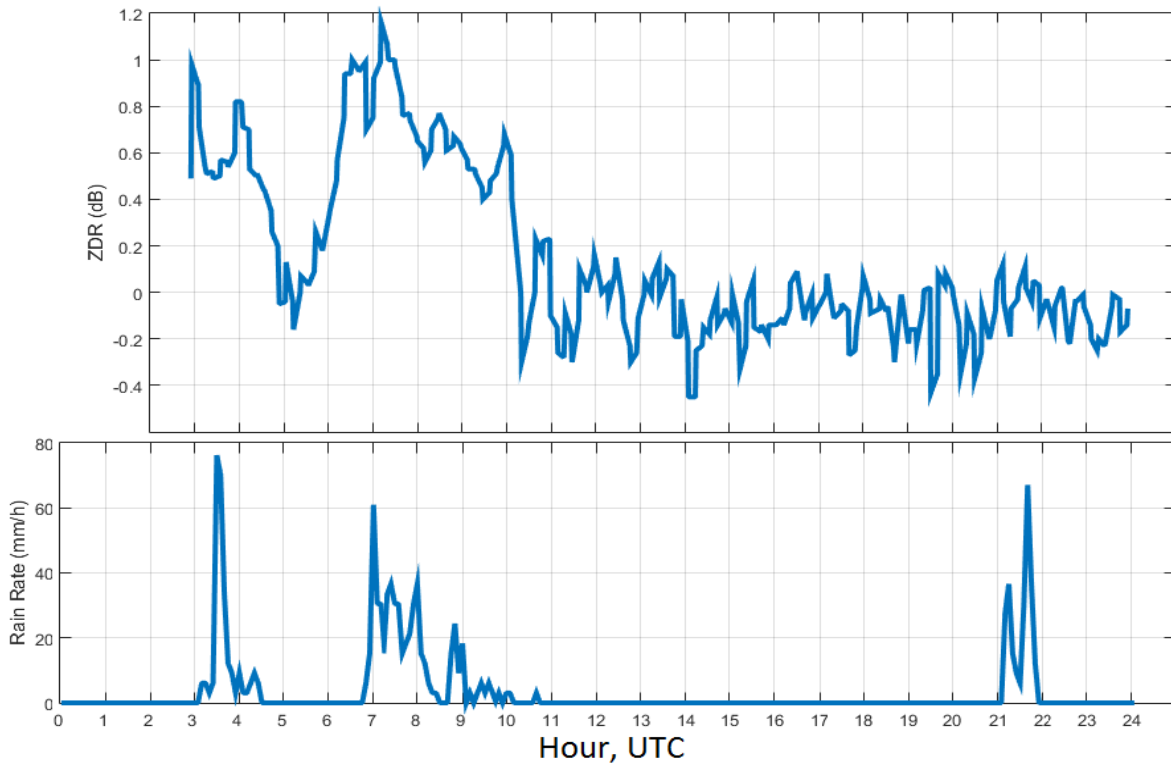

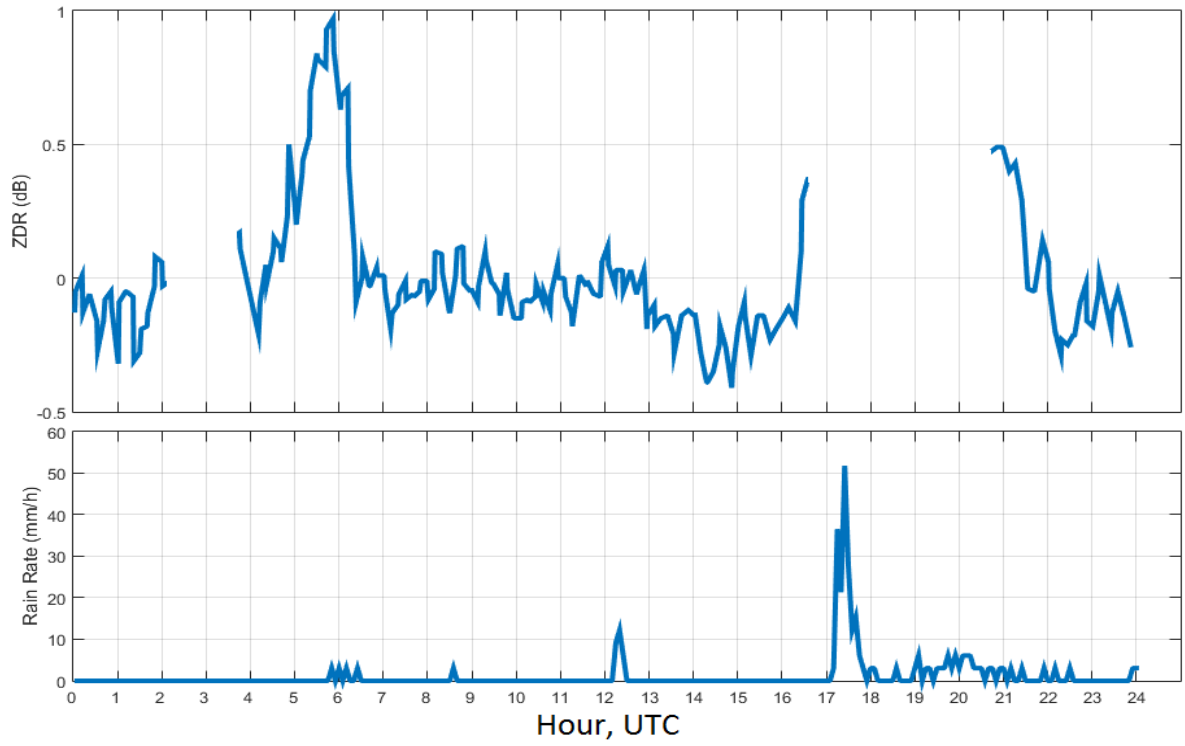*Fig. 7.4. Same as in Fig. 7.2 but on 3 July 2015.*
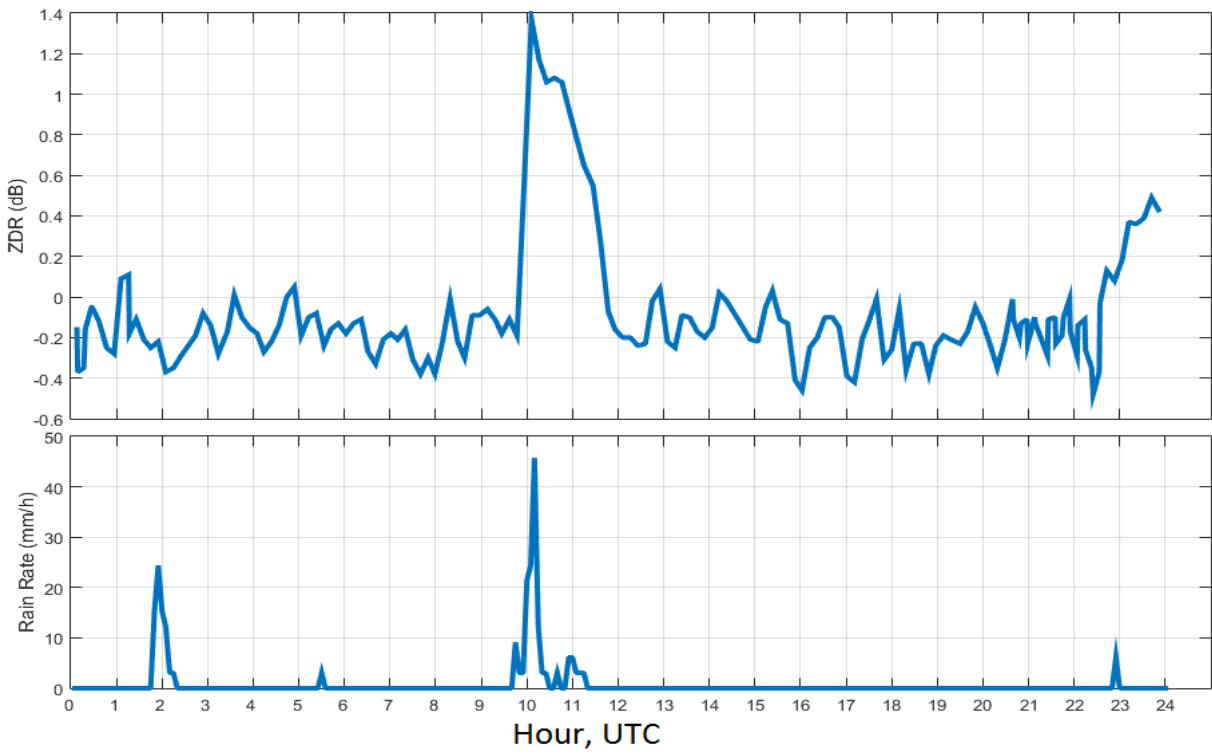
Fig. 7.5. Same as in Fig. 7.2 but on 7 July 2015.
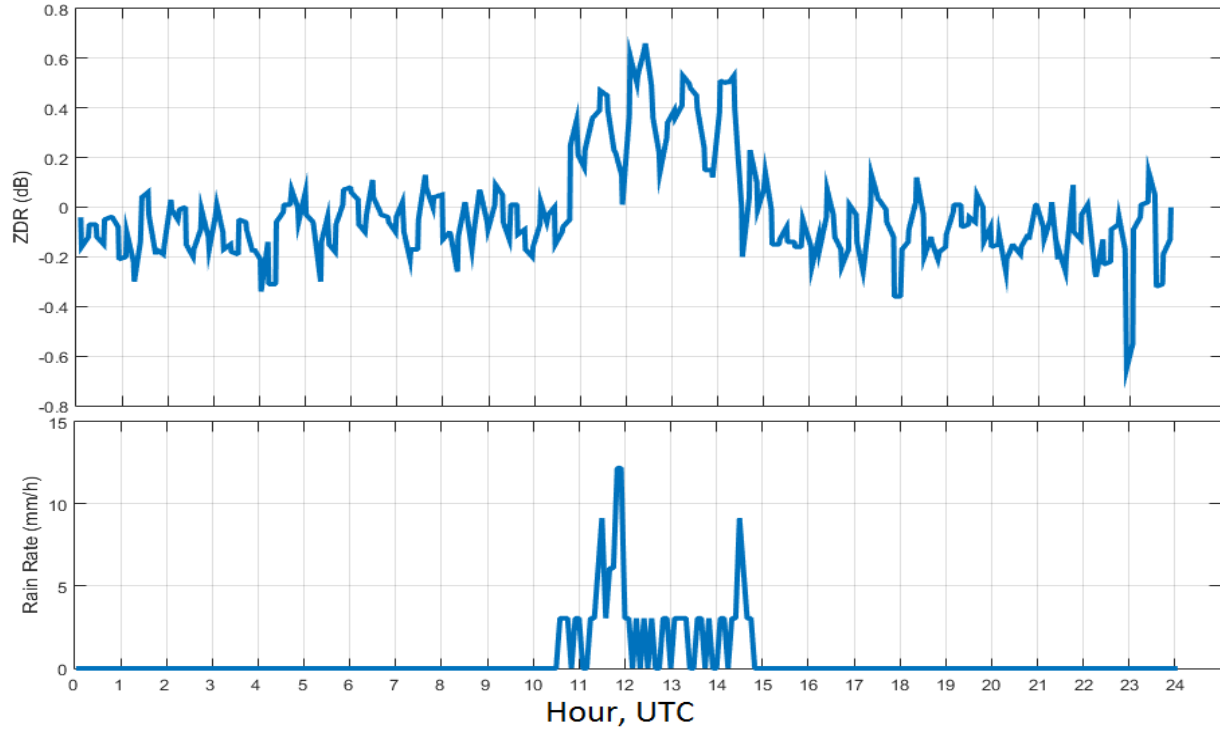

Fig. 7.6. Same as in Fig. 7.2 but on 21 July 2015.
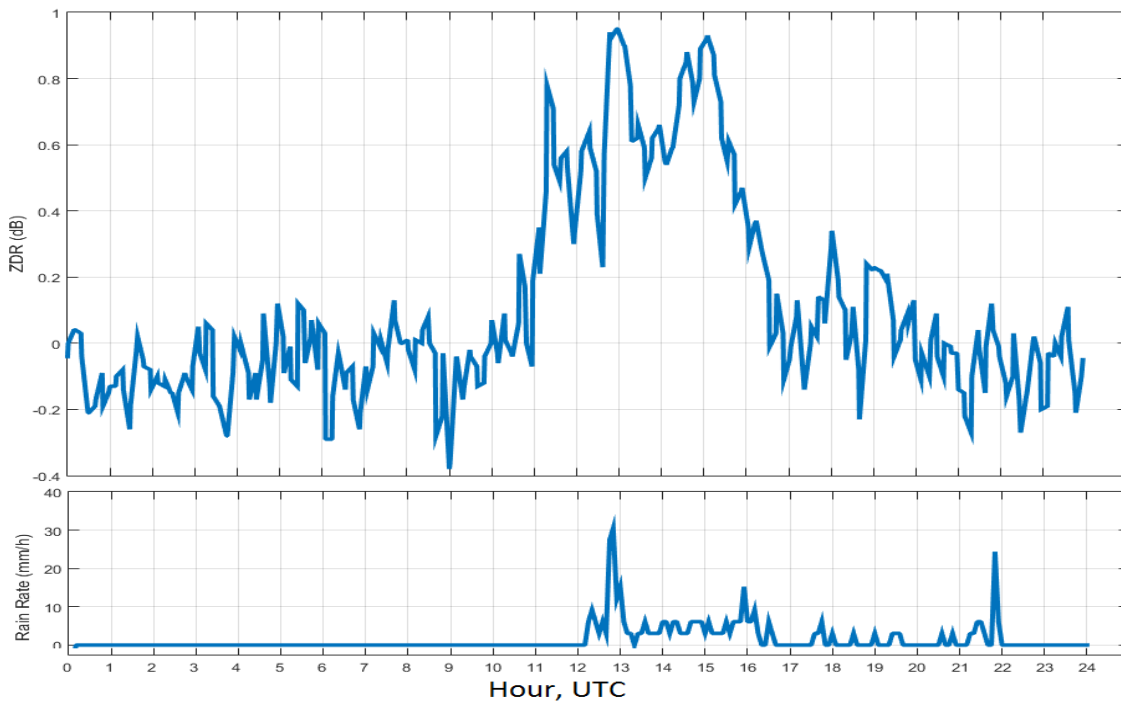
26

Fig. 7.7. Same as in Fig. 7.2 but on 4 August 2015.

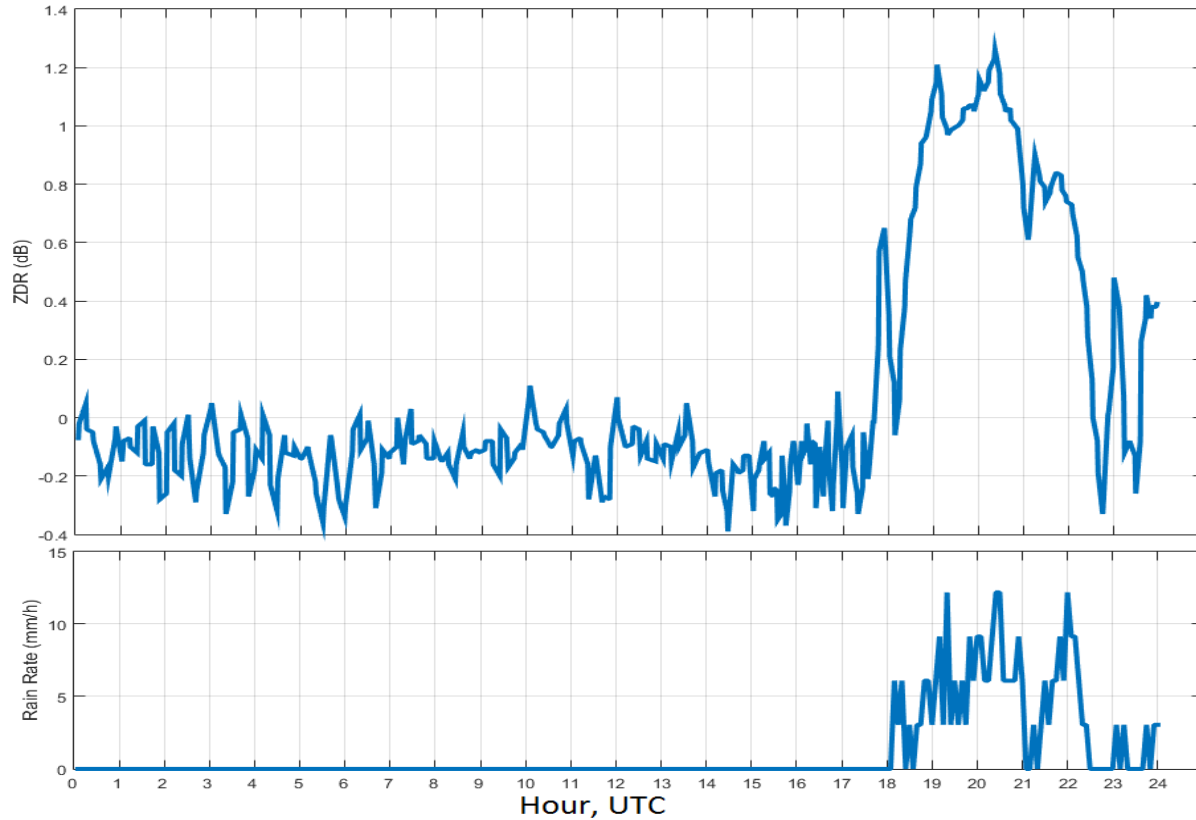*Fig. 7.8. Same as in Fig. 7.2 but on 20 September 2015.*

27

Fig. 7.9. Same as in Fig. 7.2 but on 22 October 2015.

Monitoring Z_{DR} from ground clutter could be used to determine wetness of the radome and possibly correct the effects of its differential attenuation on Z_{DR}.

It is seen in Fig. 7.1 that the mean Z_{DR} values from ground clutter are slightly different for the long and short pulses: in the short pulse mode, the mean Z_{DR} is about 0.1 dB lower than that in the long pulse mode. This should be taken into account in an operational monitoring of the system Z_{DR}.

No influence of the wind, humidity, or temperature on the mean Z_{DR} in ground clutter have been noticed. An example is in Fig. 7.10, where Z_{DR} was not averaged over 1 hour and thus has larger variations than those in Fig. 7.1.
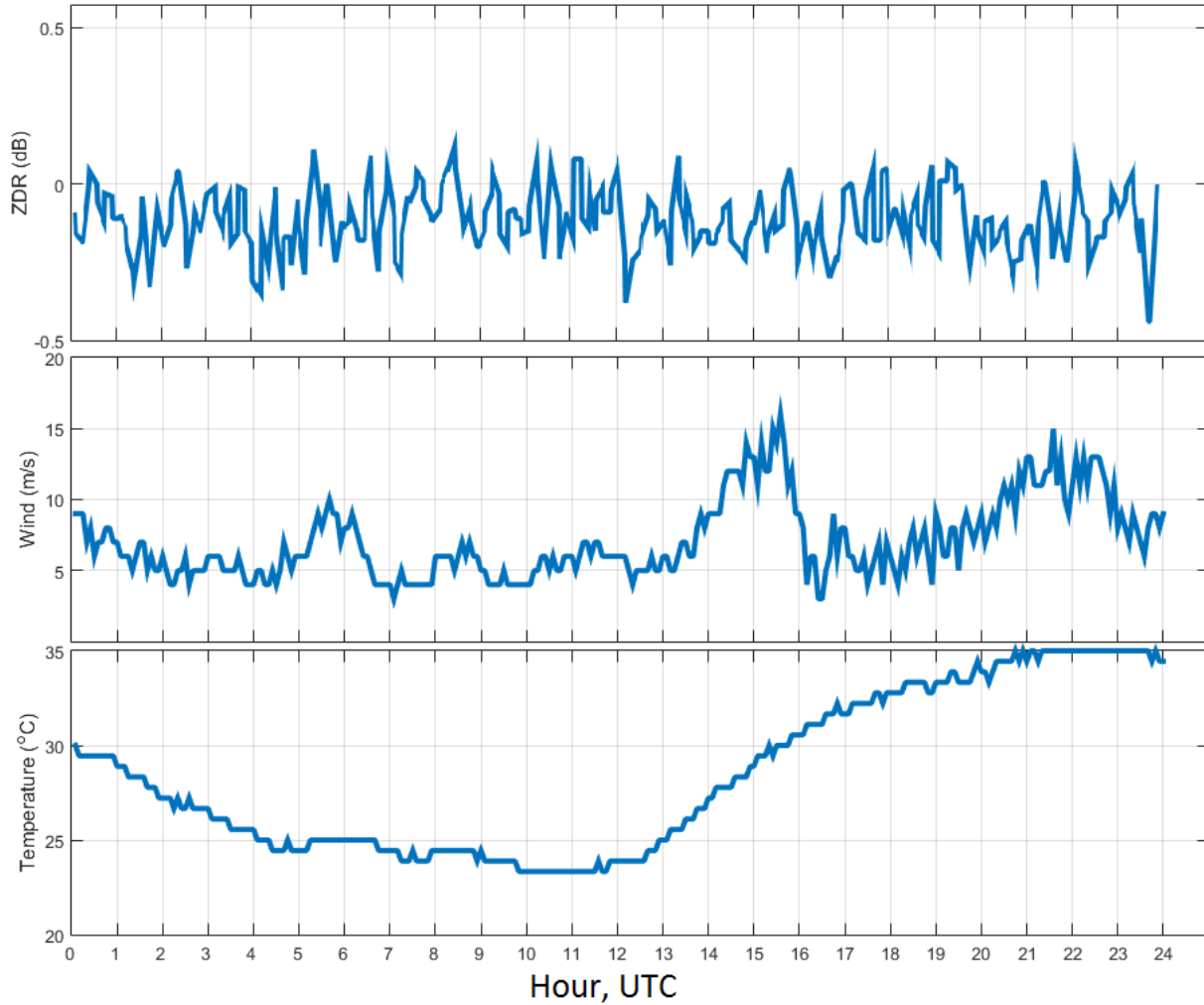
Fig. 7.10. Z_{DR} values of ground clutter (top panel), the wind velocity (central panel) and temperature (bottom panel) from Mesonet site NORM at a height of 10 m on 5 August 2015.

Sometimes variations in Z_{DR} from ground clutter have been observed in fair weather as the an example in Fig. 7.11 illustrates. Note a drop in Z_{DR} in panel (a) at $0000 - 0240$ UTC and then its rebound to the mean value. The Z_{DR} values in the panel have not been averaged over 1 hour. Note also quite synchronous changes in SNR from ground clutter (panel b) except at the indicated time interval. Such variations should be tolerated by the system, i.e., some system parameters in the technical log should reflect such variations, and the system Z_{DR} should be adjusted automatically. The main technical system parameters for the day are shown in panels (c) and (d). Panel (c) presents the transmitted powers in the channels and panel (d) shows the system biases measured by the system. No variations that can be responsible for the Z_{DR} drop in panel (a) are seen. The technical parameters in panels (c) and (d) are quite stable at 0000-0400. Such events need to be analyzed further.
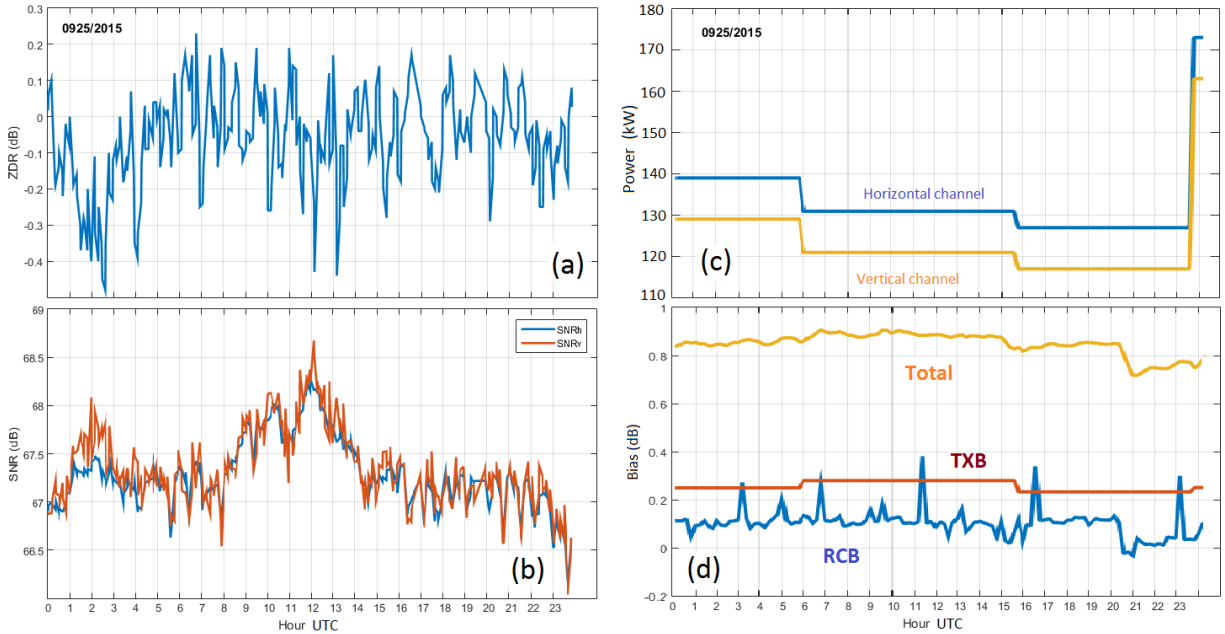
Fig. 7.11. (a): Z_{DR}, (b) SNR from ground clutter observed on 25 September 2015. The transmit powers and system Z_{DR} biases are in panels (c) and (d). WSR-88D KOUN.

8. Z_{DR} from ground clutter and Bragg scatter

Areas of Bragg scatter in the atmosphere can be used to estimate Z_{DR} system bias. It is known that Z_{DR} from Bragg scattering is close to 0 dB (e.g., Melnikov t al 2001, Ice et al. 2014) so if measured Z_{DR} in Bragg areas deviates from 0 dB, this deviation can be used to measure the system Z_{DR} bias. It is of interest to compare Z_{DR} values from Bragg scatter with the ones from ground clutter. Fig. 8.1 shows Z_{DR} values obtained from ground clutter using the Golay and median filters (the lines) versus those measured in areas of Bragg scatter (the red circles). The accuracy of the Bragg scatter measurements is about ±0.1 dB and the boundaries of the uncertainties are indicated in the figure with squares and diamonds. One can see that Z_{DR} values obtained from ground clutter using the Golay filter are close to the values obtained in areas of Bragg scatter. Thus in case of KOUN, the ground clutter signals can be used to monitor the system stability. Whether or not this is applicable to other radar sites needs to be established. Various orography could produce different relations between Z_{DR} from Bragg scatter and ground clutter. But once measured this relation could be used to monitor the system status.
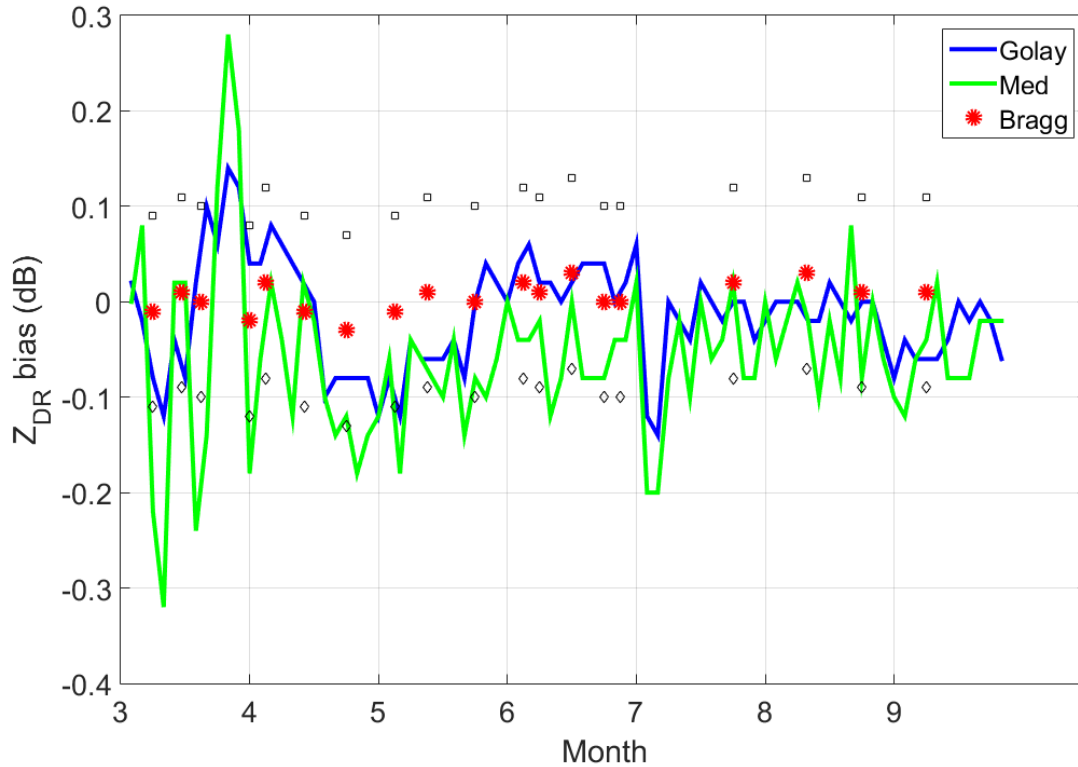
30

Fig. 8.1. Z_{DR} values from ground clutter obtained with Golay (the blue line) and median (the green line) filters and those obtained from Bragg scatter (the red circles). The uncertainties of Z_{DR} measurements using Bragg scatter are shown with the diamond (the low bound) and squares (the high bound). WSR-88D KOUN, 2014, RVP8 processor.

9. Conclusions

Returned radar signals from the ground at stationary antenna exhibit the properties valid for signals with very small number of independent samples. For the number of samples of about 64, all samples are highly correlated. Z_{DR} values from ground clutter lie in a wide interval from -25 dB to 25 dB and the correlation coefficient ρ_{hv} can be of values equal to that for weather objects. Moving antenna strongly decorrelates the signal and makes it possible to distinguish weather and ground echoes. This occurs because the terrain is strongly non-uniform.

Radar signal from the ground has been processed to establish its feasibility for monitoring of reflectivity and differential reflectivity. The processing consists of the Fourier transformations, selecting 3 central spectral lines, and computing Z_h, Z_{DR} and SNR from these It has been found that the mean Signal-to-Noise Ratio (SNR) and the maximum of Z_{DR} distributions, averaged over 1 hour, can be used for monitoring the system stability. The mean SNR in the horizontal and vertical channels are within ±1 dB and Z_{DR} is within ±0.1 dB if the system is in a good shape and

there is no rain within 50 km from radar. Such stability has been observed during time intervals from a few hours to several days.

The wind near the ground, air humidity, environmental temperature, and vegetation do not affect the Z_{DR} values measured in signals from the ground clutter. These measurements can be taken in the long and short pulse radar mode. In the short pulse mode, the mean Z_{DR} value in ground clutter is 0.1 dB lower than that measured in the long pulse mode. Temperature variations in the AME enclosure, where the receivers reside, of $0.5^{\circ}C$ lead to 0.5 dB variations in SNR and 0.1 dB variations in Z_{DR} measured from ground clutter. These variations leave SNR (reflectivity) and Z_{DR} inside tolerable changes.

Simultaneous measurements of Z_{DR} in ground clutter and in areas of Bragg scatter are consistently within 0.1 dB for the KOUN site. This also speaks for the feasibility of monitoring Z_{DR} using ground clutter.

In situations when rain is present within 50 km from radar, Z_{DR} values in ground clutter increase. A water film on the radome can decrease SNR from ground clutter by 5 dB and increase Z_{DR} by 1 dB. This should be studied further to assess the effect on the Z_h and Z_{DR} measurements.

Two unknowns in the studied procedure are:

- Very good agreement between the Z_{DR} values from ground clutter and from Bragg scatter is achieved on the WSR-88D KOUN located in central Oklahoma. For other radar sites with different orography, this agreement should be checked out.

- The WSR-88Ds operate in a 300 MHz wide frequency band. The dependence of the measurements on the carrier frequency in this band should be established. This can be done by comparing results obtained with KOUN (2705 MHz) and with practically collocated KCRI (2995 MHz).

These issues are not major obstacles for implementing the technique on the WSR-88D network. If there are dependences of Z_{DR} from ground clutter upon radar frequency and types of terrain, this difference is expected to be constant over time and can be used for the monitoring of system stability.

Recommendations.

- Verify the technique on a radar with different frequency.
- Examine data from shorter ranges and higher SNRs as thresholds to get potentially better stability of Z_{DR} from ground clutter.
- Study influence of rain water on the radome on Z_{DR} measurements from ground clutter and precipitation.
- Examine short term variations (a few hours) of Z_{DR} from ground clutter and radar system parameters that could be responsible for the variations.
- Quantify use of the single spectral line at 0 Doppler for isolating ground clutter.
- Outline to the Radar Operation Center the implementation of signal processing for monitoring ground clutter into RDA software.

Acknowledgment

References

Atlas, D., 2002: Radar Calibration: Some Simple Approaches. *Bull. Amer. Meteor. Soc.*, **83**, 1313–1316.

Billingsley, J., 2002: Low Angle Radar Land Clutter: Measurements and Empirical Models. William Andrew, Inc., 703 pp.

Bringi, V. N., and V. Chandrasekar, 2001: *Polarimetric Doppler Weather Radar. Principles and Applications.* Cambridge University Press. 636 pp.

Borowska, L. and D. Zrnic, 2012: Use of Ground Clutter to Monitor Polarimetric Radar Calibration. *J. Atmos. Oceanic Technol.*, **29**, 159–176.

Cunningham, J.G., W. D. Zittel, R. Lee, and R. L. Ice, 2013: Methods for identifying systematic differential reflectivity (ZDR) biases on the operational WSR-88D network. 36th Conf. Radar Meteor. AMS, Breckenridge, CO. Online at: https://ams.confex.com/ams/36Radar/webprogram/Paper228792.html

Curtis, C. D., 2009: Exploring the capabilities of the agile beam phased array weather radar. Ph. D. Dissertation. University of Oklahoma, XXX pp.

Delrieu, G., S. Caoudal, and J. D. Creutin, 1997: Feasibility of using mountain return for the correction of ground-based X-band weather radar data. *J. Atmos. Oceanic Technol*., 14, 368–385.

Doviak, R.J., and D. S. Zrnic, 2006: *Doppler radar and weather observations*, 2nd ed., Academic Press, 2006. 562 pp.

Fabry, F., 2004: Meteorological value of ground target measurements by radar. *J. Atmos. Oceanic Technol.*, **21**, 560–573.

Frech, M., 2013: Monitoring the data quality of the new polarimetric weather radar network of the German Meteorological Service. 36th Conf. Radar Meteorol., Breckenridge, CO. Available online at: https://ams.confex.com/ams/36Radar/webprogram/Paper228472.html

Gorgucci, E., G. Scarchilli, and V. Chandrasekar, 1999: A procedure to calibrate multiparameter weather radar data using the properties of the rain medium. *IEEE Trans. Geosci. Remote Sens.*, **17**, 269–276.

Hoban, N.P., J. G. Cunningham, and D. Zittel, 2014: Estimating Systematic WSR-88D Differential Reflectivity (ZDR) Biases Using Bragg Scattering. *30th Conf. Environmental Information Processing Technologies.* AMS, Atlanta. Online at: https://ams.confex.com/ams/94Annual/webprogram/Paper237404.html

Hubbert J., M. Dixon, S. Ellis, and G. Meymaris, 2009: Weather radar ground clutter. Part I: Identification, modeling, and simulation. *J. Atmos. Oceanic Technol.*, 26, 1165–1180.

Ice, R.L., A. K. Heck, J. G. Cunningham and W. D. Zittel, 2014: Challenges of polarimetric weather radar calibration. ERAD 2014 - The Eighth European Conf. Radar Meteorol. Hydrology, Germany. Online at: http://www.pa.op.dlr.de/erad2014/programme/ExtendedAbstracts/117_Ice.pdf

Kulemin, G.P, 2003: *Millimeter-Wave Radar Targets and Clutter.* Artech House, 327 pp.

Lee, J-S., and E. Pottier, 2009: *Polarimetric Radar Imaging: from basics to application.* CRC Press, New York, 357 pp.

Long, M. W., 2001: *Radar Reflectivity of Land and Sea.* Artech House, 534 pp.

Melnikov, V., and D. Zrnic, 2004: Simultaneous Transmission Mode for the Polarimetric WSR-88D, NOAA/NSSL Report, 84 pp. Online at: http://www.nssl.noaa.gov/publications/wsr88d_reports

Melnikov, V.M., R. J. Doviak, D. S. Zrnic, and D. J. Stensrud**,** 2011: Mapping Bragg scatter with a polarimetric WSR-88D. *J. Atmos. Oceanic Technol.,* **28,** 1273-1285.

Melnikov, V., D. Zrnic, M. Schmidt, and R. Murnan, 2013: Z_{DR} calibration issues in the WSR-88Ds. NSSL interim report, 54 pp. Online: http://www.nssl.noaa.gov/publications/wsr88d_reports/WSR88D_ZDRcalib_Report_2013.pdf

Meneghini, R., and T. Kozu, 1990: *Spaceborn Weather Radar.* Artech House, 197 pp.

Middleton, D., 1960: *Statistical Communication Theory.* McGrawHill, 1140 pp.

Pellarin, T., G. Delrieu, and J. D. Creutin, 1999: Variability of mountain returns during dry-weather conditions: Applications to radar calibration control. Preprints, 29th Conf. on Radar Meteorology, Montreal, QC, Canada, Amer. Meteor. Soc., 772–775.

Rinehart, R. E., 1978: On the use of ground return targets for radar reflectivity factor calibration checks. *J. Appl. Meteor*., **17**, 1342–1350.

Schaffner, M., P. L. Smith, K. R. Hardy, and K. M. Glover, 1975: Comments on ''Applications of radar to meteorological operations and research.'' *Proc. IEEE*, **63**, 731–733.

Sugier, J., and P. Tabary, 2006: Evaluation of dual polarization technology at C-band for operational weather radars as part of the EUMETNET OPERA program. 4th European Conf. Radar Meteorol. Hydrolog., Barcelona, Spain. http://www.crahi.upc.edu/ERAD2006/proceedingsMask/00010.pdf

Vaisala Co., 2014: Meteorological Solutions Worldwide. http://www.vaisala.com/en/meteorology/products/weatherradars/Pages/default.aspx

Vukovic, Z.R., J. M. C. Young, and N. Donaldson, 2015: An operational use of ground clutter to monitor radar performance. 37th Conf. Radar Meteorol. AMS, Norman, OK. Available online at: https://ams.confex.com/ams/37RADAR/webprogram/Paper275669.html

Williams, E., K. Hood, D. Smalley, M. Donovan, V. Melnikov, D. Forsyth, D. Zrnic, D. Burgess, M. Douglas, J. Sandifer, D. Saxion, O. Boydstun, A. Heck, and T. Webster, 2013: End-to-end calibration of Nexrad differential reflectivity with metal spheres. 36th Conf. Radar Meteor. AMS, Breckenridge, CO. Online at: https://ams.confex.com/ams/36Radar/webprogram/Paper228796.html

Wallace, P.R., 1953: Interpretation of the fluctuating echo from randomly distributed scatterers. *Can J. Physics*, **31**, 995-1009.

Zhang, J., K. Howard, C. Langston, S. Vasiloff, B. Kaney, A. Arthur, S. Van Cooten, K. Kelleher, D. Kitzmiller, F. Ding, D-J. Seo, E. Wells, C. Dempsey, 2011: National Mosaic and Multi-Sensor QPE (NMQ) System: Description, Results, and Future Plans. Bull. Amer. Meteor. Soc., 92, 1321-1338.

Zrnic, D., V. Melnikov and A. Ryzhkov, 2006a: Correlation coefficients between horizontally and vertically polarized returns from ground clutter. *J. Atmos. Oceanic Technol.*, **23**, 381–394.

Zrnic D.S., V. M. Melnikov, and J. K. Carter, 2006b: Calibrating differential reflectivity on the WSR-88D. *J. Atmos. Ocean. Technol*., **23**, 944-951.